ABSTRACT

STOKELY, MATTHEW H. Deployment, Testing and Analysis of Advanced Thermosyphon Target Systems for Production of Aqueous [^{18}F]Fluoride via $^{18}O(p,n)^{18}F$. (Under the direction of Dr. J.Michael Doster.)

Single phase and boiling batch water targets are the most common designs for the cyclotron production of ^{18}F via the $^{18}O(p,n)^{18}F$ reaction. Thermosyphon targets have design and operating characteristics which enable higher power operation than conventional boiling targets of like size. Experimental thermosyphon target systems demonstrated the feasibility of high intensity irradiation via bottom pressurized operation. An effective experimental characterization platform was developed and utilized in parallel with computational modeling efforts to further improve designs. A control strategy was also developed to provide a simple and robust means of remote target operation. Clinical production systems were designed and deployed at two facilities.

Deployment, Testing and Analysis of Advanced Thermosyphon Target Systems for
Production of Aqueous [^{18}F]Fluoride via ^{18}O(p,n)^{18}F

by
Matthew Hughes Stokely

A dissertation submitted to the Graduate Faculty of
North Carolina State University
in partial fulfillment of the
requirements for the Degree of
Doctor of Philosophy

Nuclear Engineering

Raleigh, North Carolina

2008

APPROVED BY:

_____	_____
Dr. J. M. Doster	Dr. M. Bourham
Chair of Advisory Committee	
_____	_____
Dr. B. Wieland	Dr. G. Bida

_____
Dr. M. Shearer

BIOGRAPHY

Matthew Hughes Stokely was born October 28, 1980 to Amelia and Joseph Stokely. He attended primary and high school in the small, backwoods town of Chapel Hill, North Carolina. In 1998, he began undergraduate work at North Carolina State University. In 2003, he graduated with a bachelor's degree in Electrical Engineering. After a short career as a riverboat captain in Tennessee, he returned to NCSU to pursue a graduate degree in Nuclear Engineering. In 2008, he completed his Ph.D.

ACKNOWLEDGEMENTS

I would first like to acknowledge all of the support provided by my committee members. Dr. J. Michael Doster has been an outstanding instructor, advisor and friend during my years in Raleigh. Dr. Gerald Bida has been an invaluable source of insight and a model of organization and professionalism. Dr. Bruce Wieland is one of the best people anyone could ever hope to know, personally or professionally.

I also owe many thanks to my fellow graduate students for their help and support along the way. These people include, in no particular order, Jonny Waldes, Will Wieselquist, Ross Hays, Matt Jessee, Bobby Newnam, Johanna Peeples, Mark Humphrey and Loren Roberts.

The bulk of my research was performed at cyclotron facilities, and I relied heavily on site engineers and operators who worked countless extra hours to accommodate experiments. Thank you Shawn Murphy and Michael Daly, the stewards of the Duke CS-30. At the Milwaukee Medical Cyclotron, success would not have been possible without the efforts of Jerry Rasmussen and Roger Smith. I would also like to thank Dr. James Lamb, president of Cyclomedical Applications Group, for providing a first class test site.

I cannot thank my parents and family enough for supporting and encouraging me during my decade long college career. I would never have come this far without them placing so much value on my education.

Finally, I want to thank my girlfriend, Lori, who has supported me from the very beginning. She is a uniquely talented, beautiful and intelligent woman who I love in spite of the fact that she attended UNC Chapel Hill and ultimately became a lawyer.

TABLE OF CONTENTS

LIST OF FIGURES

LIST OF TABLES

CHAPTER 1 - INTRODUCTION

1.1 Background

Positron Emission Tomography (PET) is a functional imaging technique that can depict metabolic activity within the body. This technique is particularly useful in the detection and staging of, at present, seven different cancers and Alzheimer's disease. PET imaging utilizes compounds labeled with positron emitting radioisotopes, the most widely employed being 2-deoxy-2-[^{18}F]fluoro-D-glucose (^{18}FDG). Upon injection, the compound migrates throughout the body. Areas with high metabolic rates will, in turn, have elevated concentrations of fluorine-18 from the metabolically trapped radiopharmaceutical [17].

Fluorine-18 decays by positron emission with a half-life of 109.7 minutes. The positron has a range of only a few millimeters in tissue before it slows sufficiently to combine with an electron. The resulting annihilation produces a pair of 511 keV photons traveling in opposite directions. A fraction of these photons can be recorded using coincidence detectors and a 3-dimensional functional image can be computed [17].

The ^{18}F radionuclide is predominantly produced using an accelerator via the ^{18}O(p,n)^{18}F reaction. The target consists of either liquid $H_2^{18}O$ or gaseous $^{18}O_2$ contained in a vessel upon which high energy protons (>2.5 MeV) are incident. Minimally, the production capability of any given target system is a function of beam energy and current. Due to the relatively small cross section of the nuclear reaction, it requires roughly two thousand incident protons to produce one ^{18}F radionuclide [11]. One consequence of producing a useful inventory is the large amount of thermal power deposited in the target medium. There are many challenges presented by liquid water target systems including, but not limited to,

1

thermal hydraulic behaviors, radiation transport uncertainties, dynamic instabilities, and chemical compatibility restrictions.

While the first PET scans were performed early in the 1970s, many clinical applications of the technology were not realized for almost a decade until the synthesis of ^{18}FDG. Until the early 1990s, PET imaging facilities required an on-site cyclotron for isotope production [14]. Early [^{18}F]targets were constructed of copper, nickel plated copper and stainless steel. These systems were typically operated below saturation temperature for the target medium [12,28].

As the experience base for PET isotope production grew, the regional isotope production facility was conceived. While the first distribution center was constructed in 1991, substantial market growth occurred after 1998, when Medicare coverage expanded to include ^{18}FDG-PET scans. This resulted in the rapid and sustained rise in demand for ^{18}FDG during the years to follow [4, 7].

Three cyclotron manufacturers produced the overwhelming majority of the accelerators for the distribution center market: CTI/SIEMENS (RDS-112, RDS-111), GE (PETtrace, MINItrace), and IBA (18/9). The industry standard for [^{18}F] target technology soon became top pressurized boiling water, or reflux, systems with silver target chambers [3,18].

The design and development of [^{18}F] target systems with improved heat rejection and increased production capacity is an active area of research for several commercial PET vendors [2,8,21]. While the new generation of targets use inert wetted materials and can run at higher power levels, the basic principle of operation has not changed.

2

1.2 Purpose

One aim of this thesis was to construct, deploy, and characterize a series of thermosyphon target systems suitable for clinical production of $^{18}F^{-}$. This included component selection, fabrication of target body and control system as well as software development. Two pilot sites were chosen for beam testing, the Duke University PET Facility(DUKE) and the Wisconsin Medical Cyclotron (WMC). Both facilities produce ^{18}FDG for clinical use, but the accelerator technologies are very different. Duke operates a CS-30 four-particle, positive ion cyclotron with an extracted proton energy of 26 MeV and maximum beam current of 45 μA. WMC operates a negative ion GE PETtrace, which is configured strictly for proton operation at 16.5 MeV and maximum beam current of 150 μA. A limited amount of beam testing was also conducted at a third site using an IBA Cyclone-30.

Six prototype target designs were developed during research collaboration between the Nuclear Engineering Department at North Carolina State University and Bruce Technologies, Inc. While there are unique features associated with each design, the racetrack shaped chamber is a common trait (Figure 1-1). This geometry can be specified with three dimensions: radius, height and depth. The chamber dimensions for the prototype thermosyphon targets are listed in Table 1-1. The negative ion cyclotrons produce a larger, more uniformly distributed beam at the target than the CS-30. Because of this fact, the Duke targets have 10 mm chamber diameters while the PETtrace and Cyclone-30 targets have 13.5 mm and 15 mm chamber diameters.

3
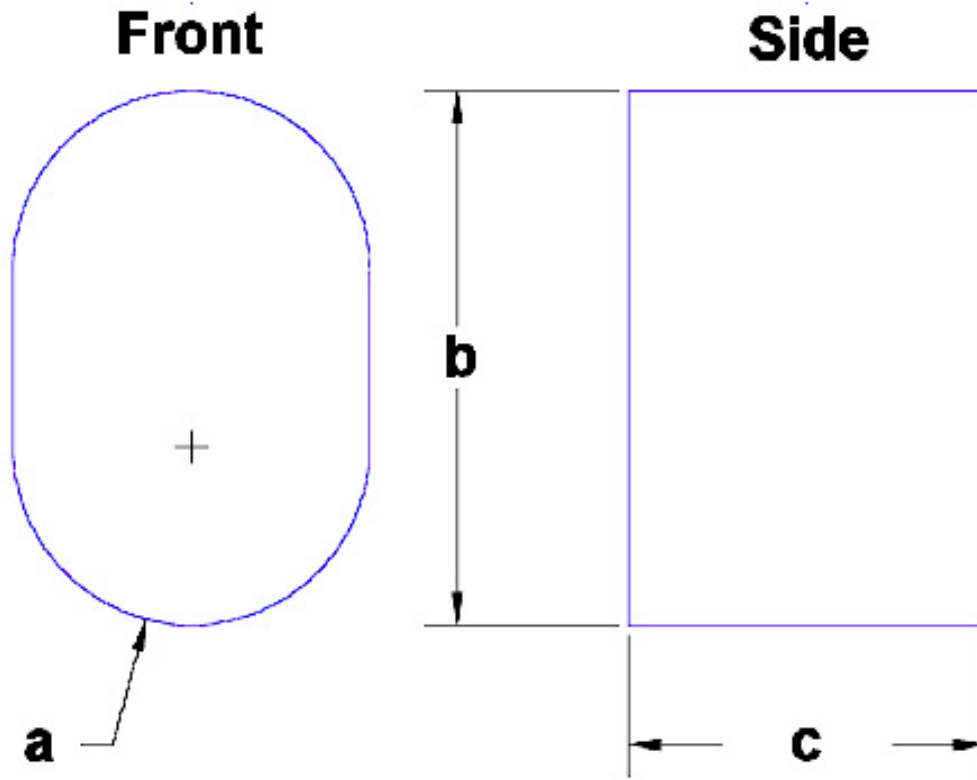
Figure 1-1: Target Chamber Dimensions

Table 1-1: Target Chamber Dimensions

Target	Radius a (mm)	Height b (mm)	Depth c (mm)	Volume (mL)	Control System
TS4-DUKE	5	20	15	2.7	1
TS4-CYC30	7.5	25	15	5.9*	1
TS4-WMC	7.5	25	15	5.9*	1
TS5-DUKE	5	15	10	1.3	1
TS6-DUKE	5	15	15	1.9	2,3
TS6-WMC	7.5	22.5	15	4.3	3
TS7-WMC	6.75	20.25	13.5	3.2	3

4

www.manaraa.com

1.3 Related Work

Bruce Technologies, Inc., and the Nuclear Engineering Department of North Carolina State University are currently developing a 15+ kilowatt recirculating target for large scale F-18 production. These target systems will likely be marketed to radiopharmaceutical distribution centers where higher yields are needed to supply [18]FDG over large distances.

The recirculating target system utilizes a regenerative turbine pump to pass target water through the beam strike at high velocity [13,29]. The waste heat is then transferred from the target water through a compact heat exchanger to the cyclotron cooling system. The advantage of this design is the ability to run at very high power densities by suppressing boiling in the target medium.

CHAPTER 2 - TARGET DESIGN REQUIREMENTS

2.1 Liquid Target Fundamentals

The function of a production accelerator target is the transmutation of a stable element into a product radionuclide via bombardment with high energy particles. The specific target geometry and implementation are the product of many disciplines including chemistry, nuclear physics, and thermodynamics. In the case of $^{18}F^-$ production, the target medium is [O-18]enriched water. A liquid target is constructed of, principally, three components:

1. A chamber containing the target medium;

2. A foil window that is strong enough to confine the medium within the chamber, yet thin enough to allow particles to pass through with an acceptable loss of energy;

3. A target body that houses the chamber and window, which connects to a beam line or port and provides a path for coolant to remove waste heat from the system.

A simplified target drawing is included to highlight these features (Figure 2-1). The target chamber shown has a racetrack shape. This has been the geometry of choice for boiling water targets since the inception of the PET cyclotron. It is intended to accommodate boiling in the lower region of the chamber, where the beam enters the target. The area above the beam strike provides a vapor space, or condenser. This geometry has been utilized in both traditional reflux and thermosyphon targets.

6
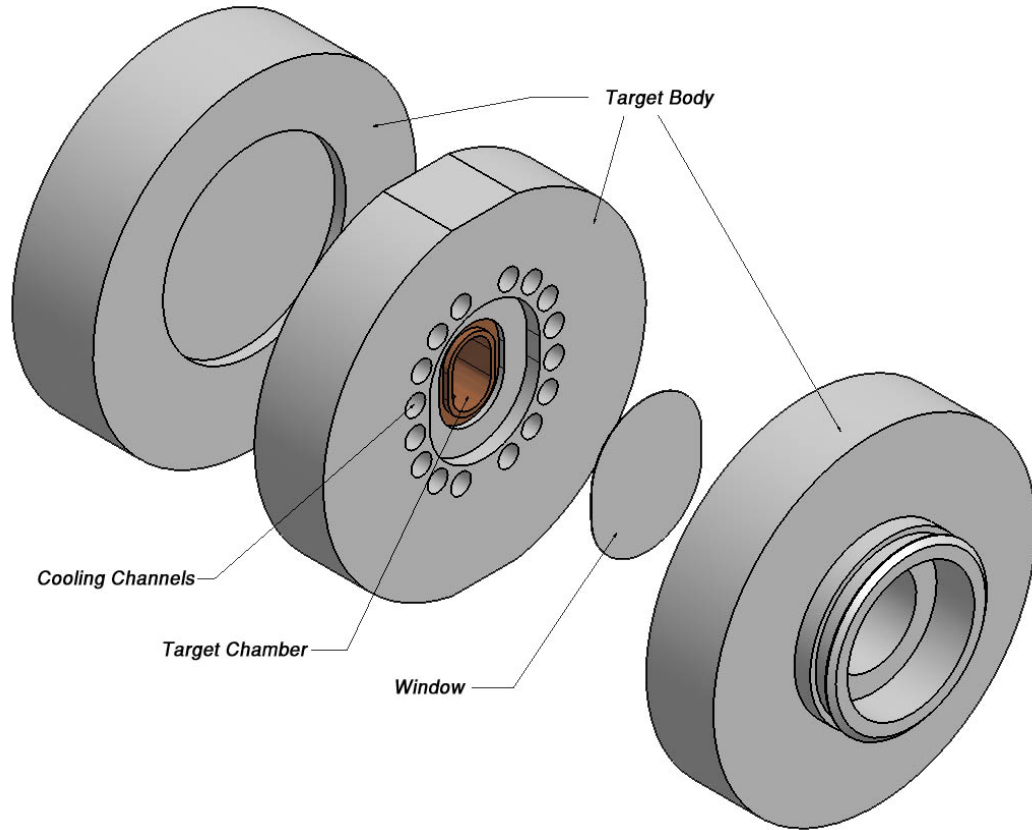
Figure 2-1: Principal Liquid Target Components

The production capacity of any target system is a function of beam energy and current. Waste heat is generated by the protons as they slow down in the target. If the heat input is greater than the thermal capacity of the system, vapor voids in the beam strike can lead to particles fully penetrating the target medium. If the protons do not stop in the target medium, but rather in the target body, radionuclide production will suffer. Consequently, the design and development of target systems with increased heat removal capabilities is one way to expand production capacity.

7

2.2 Thermosyphon Operating Principle

Reflux target systems are the industry standard in [18]FDG PET production. It is important to make the distinction between a reflux target and a thermosyphon target. Both types of targets are self-regulating, in that the vapor generated will occupy the amount of condensing surface area necessary to reject the incident beam power. The difference between the two systems lies in the manner in which the chamber is pressurized (Figure 2-2).
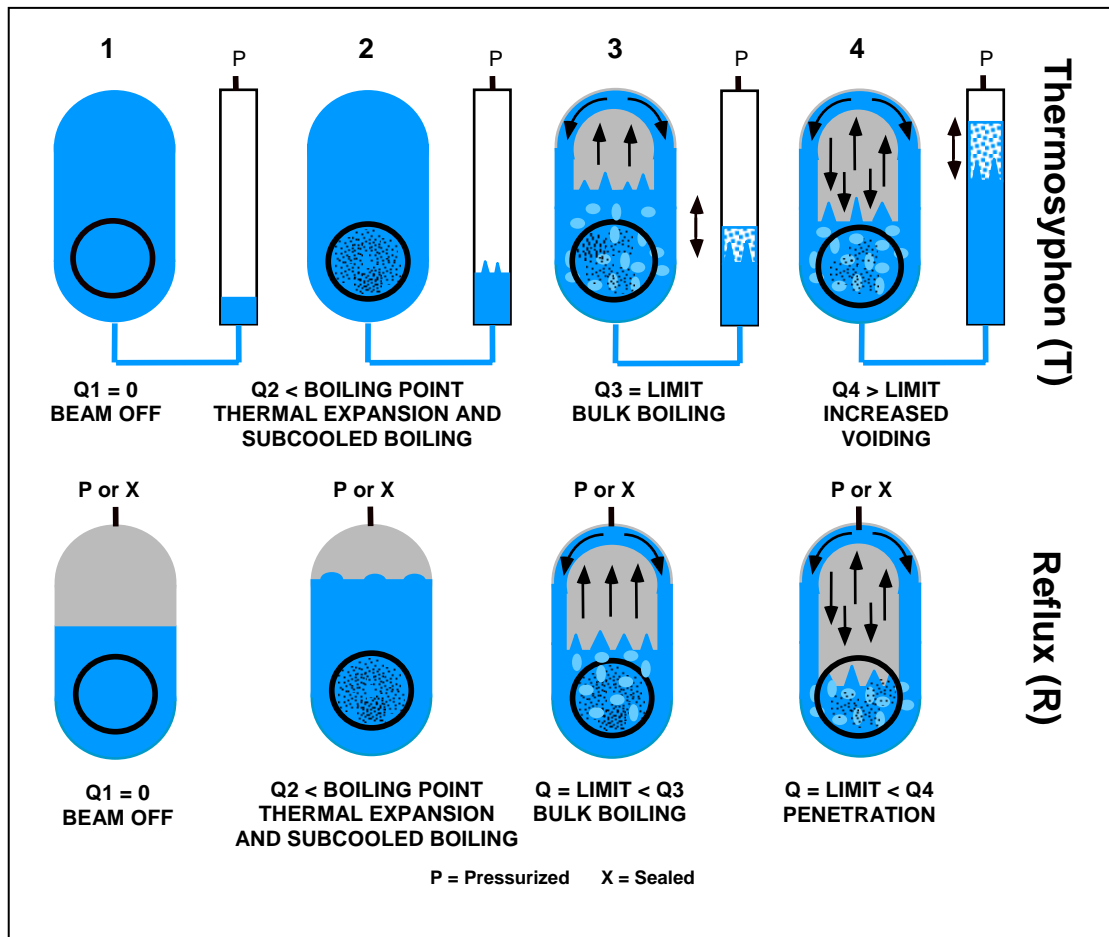
Figure 2-2: Qualitative Behavior of Reflux and Thermosyphon Targets

Reflux targets are pressurized from the top of the liquid volume. Because of this fact, there exists an initial amount of non-condensable gas which mixes with the liquid and vapor

during bombardment. Even a small component of non-condensable gas produces a dramatic increase in resistance to heat transfer at a condensing surface[5]. This is significant, as the condensing layer can become the limiting resistance as the target is cooled more aggressively.

In contrast, a thermosyphon target is initially filled completely and pressurized from the bottom via an external expansion volume. This maximizes the effective heat transfer area in the condensing region of the target volume by eliminating the presence of non-condensable gas.

2.3 Materials Selection and Fabrication

Silver and tantalum were both used for target chamber materials. Silver is less expensive not only as a raw material, but is much easier to fabricate. Fabrication of tantalum target chambers has been a challenge since the beginning of the project. Machinists at local facilities have encountered severe difficulty achieving adequate tolerances, especially with small, deep holes. The tantalum chambers for the most recent targets have been fabricated by a refractory metal specialist in Oregon. This company has the capability to produce inserts to the necessary specifications, but the process is very expensive and time consuming.

Silver has a much higher thermal conductivity, 430 W/(m*K), compared to 57 W/(m*K) for tantalum. Tantalum is more inert and results in better quality fluoride ion, as well as longer intervals between target service[21]. The use of tantalum also results in lower dose rates due to target activation than silver.

Target bodies are constructed of 6061 Aluminum. Advantages include ease of fabrication, low cost, very limited activation and high thermal conductivity. Fluoride ion

9

readily attaches to aluminum surfaces, however, so the wetted components outside the chamber are constructed of 300 series stainless steel.

Havar[TM][9] foil is used for target windows in all targets. A nominal thickness of 0.001" is typically used. In some instances for the PETtrace targets, which have unsupported window radii of 13.5 mm and 15 mm, a 0.002" thick foil was used to provide additional pressure margin. Window materials less strong than Havar can be used with a support grid. Grids reduce beam transmission and were not needed to increase pressure margin in these targets.

CHAPTER 3 - TARGET INSTRUMENTION AND CONTROL

3.1 Control System Requirements

The thermosyphon target must be loaded and pressurized from the bottom of the beam strike, which requires more control valves and operating states than a conventional reflux target system. Additionally, while the cost of [O-18]enriched material is currently much lower than in the past, consistent fill volumes should be maintained to manage raw material consumption.

The target area in any accelerator is a high radiation environment, especially during irradiation. It is imperative to have a highly robust and reliable system to remotely control the target system components. In many cases, dose rates in proximity of the target restrict human intervention. Component failures can interrupt production and in the worst instances result in extended downtimes.

A PC-based control system was developed to remotely operate the target control system and record transducer data. This system has three principal components: controller, target filler and helium supply system.

National Instruments(NI) LabView software and NI FieldPoint hardware were selected for the controller based on a combination of versatility, ease of implementation, adaptability and low cost. The same controller platform (Figure 3-1) was used for all target systems, while the helium delivery system was redesigned once during the course of the

11

project and the target filler was redesigned twice. This resulted in three distinct versions of the control system.
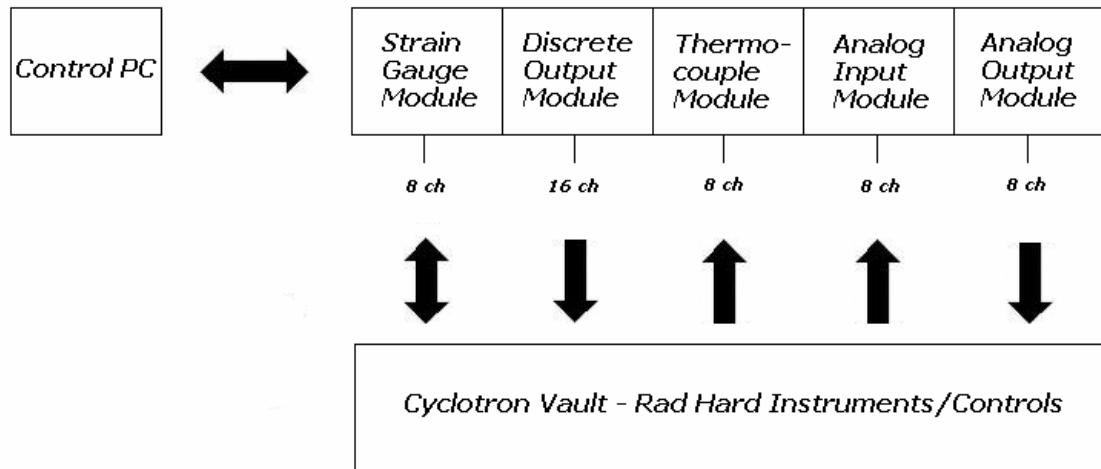
Figure 3-1: Field Point Hardware Hierarchy

Control PC – Runs the system software. Communicates with the FieldPoint modules via RS-232 or RS-485 serial protocol.

Strain Gauge Module – Provides both excitation and input for strain gauge type pressure transducers. Transducers of this type with no intrinsic signal conditioning perform better in high radiation environments.

Discrete Output Module – Energize discrete state devices such as solenoid valves, single speed motors or pumps.

Analog Input Module – Interfaces with conventional loop current transducers and reads beam current reference signal.

12

While the control system implementation has evolved over the course of the project, the overall strategy has remained the same. The following section illustrates the key concepts of thermosyphon target control.

3.2 Target Control Strategy

The target chamber and expansion volume are initially sealed after being purged with helium. The loading reservoir is filled with target water.
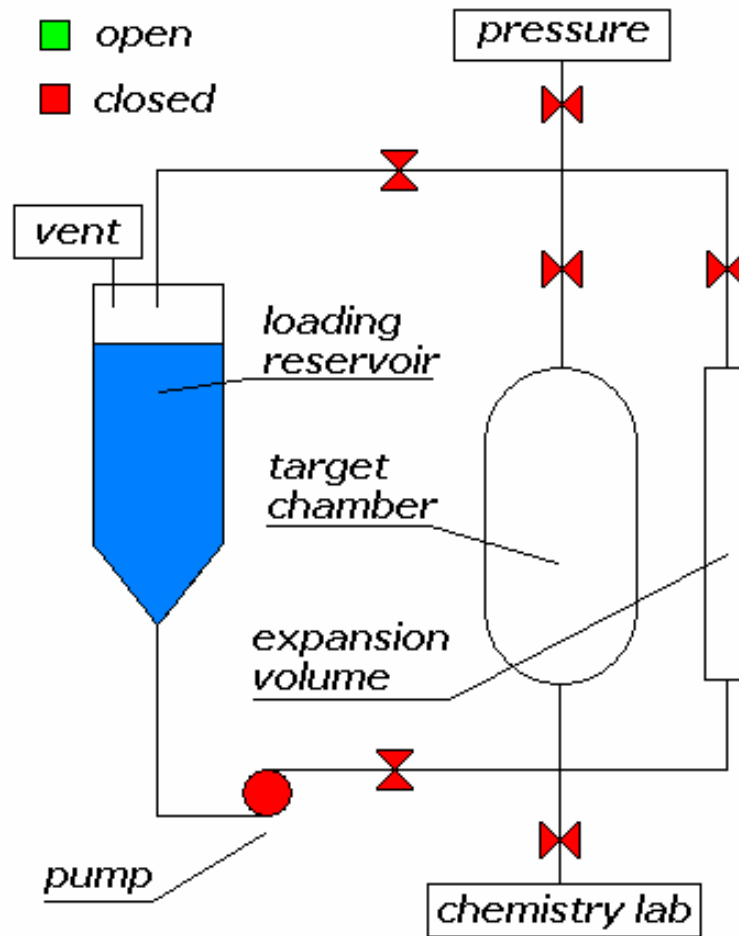
Figure 3-2: Target Operation State 1 of 5

13

The loading valves open and the pump begins to fill the target chamber. The path to the expansion volume is open, but the top valve is closed so very little fluid enters the expansion volume initially.
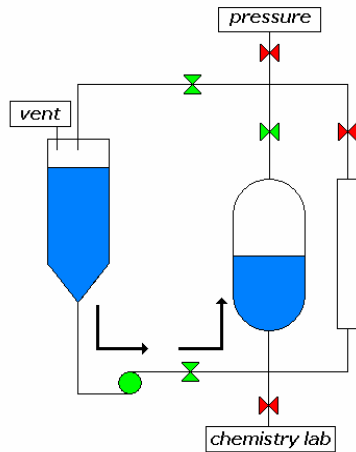
Figure 3-3: Target Operation State 2 of 5

After the target chamber fills completely, fluid returns to the loading reservoir and a circulating flow is established. The pressure at the bottom of the target chamber increases and pressurizes the gas in the expansion volume, allowing fluid to enter.
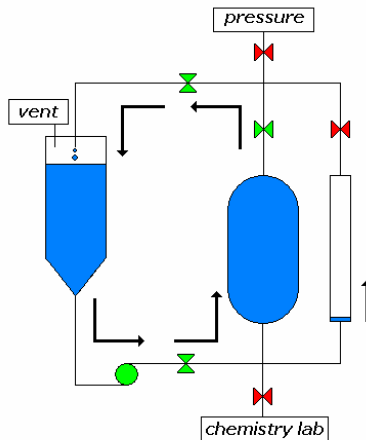
Figure 3-4: Target Operation State 3 of 5

14

Once the pressure in the expansion volume reaches equilibrium with the pressure generated by the circulating flow, the loading valves are closed and the expansion chamber is connected to a pressure source from above. The beam is then incident upon the target chamber for the duration of the irradiation.
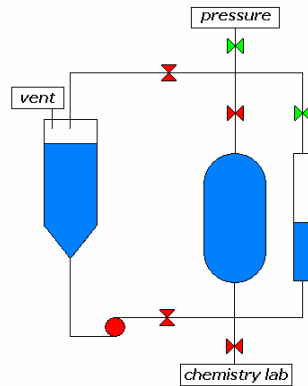
Figure 3-5: Target Operation State 4 of 5

When the irradiation is complete, the target chamber is emptied by applying pressure from above. The irradiated water is delivered to a synthesis unit in the chemistry lab or simply to a dose calibrator. The water in the expansion chamber is recovered afterwards, rinsing any residual activity from the delivery line.
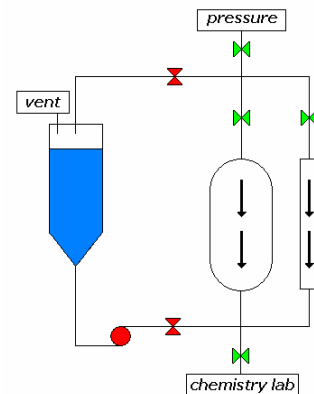
Figure 3-6: Target Operation State 5 of 5

15

3.2 Control System 1.0

The first experimental platform utilized a motor driven 3-way ball valve system in the target filler to perform fluidic switching during target operation. The helium supply system consisted of three fixed pressure regulators and a vent line each with individual 24 volt solenoid valves. A metering pump was used for moving liquid through the target during the load sequence. Target pressure was monitored by an internal piezoelectric transducer in the base of the chamber flange. A schematic of this system is included in Figure 3-7.
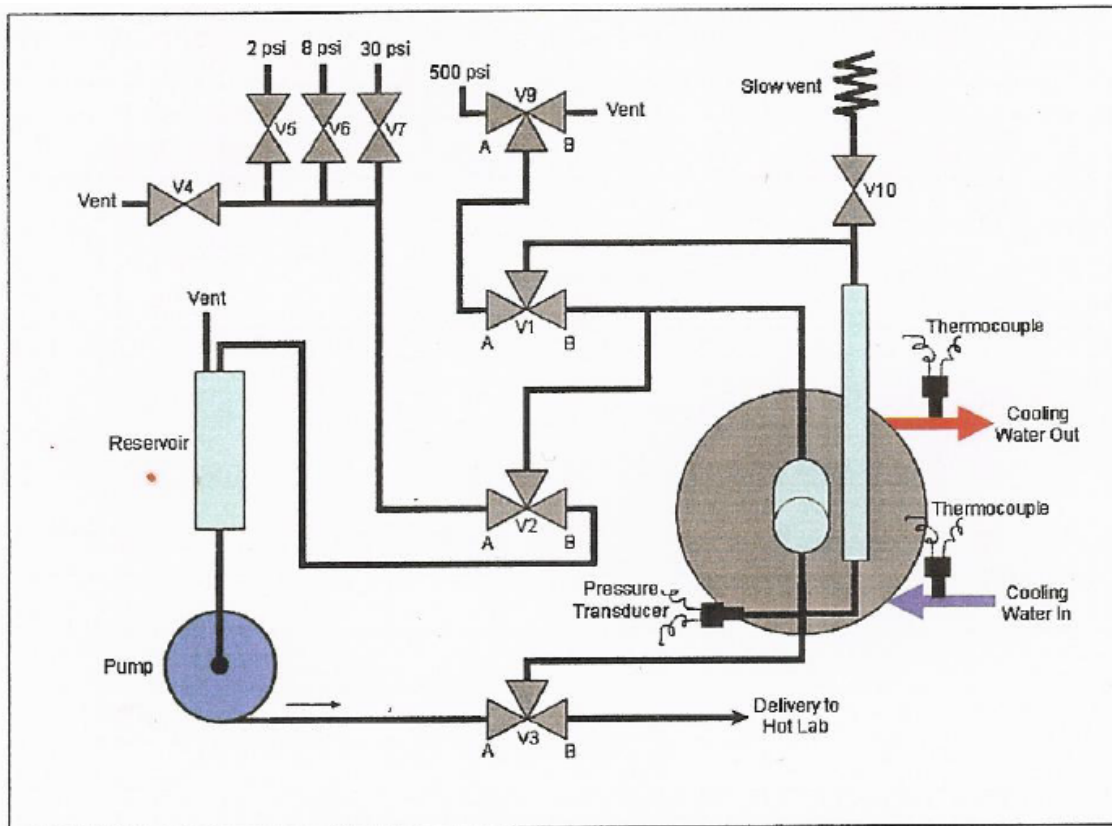
Figure 3-7: System 1.0 Schematic

While this system was used for several years to collect experimental data, it became far too problematic for use in clinical production. The typical frequency for component

16

failure leading to downtime was on the order of two per month. These failures included radiation damage to the pressure transducer, ball valves leaking past the shaft seal, ball valves failing to make position and solenoid valve temperature fatigue.

The motor drives (Figure 3-8) cycled the valve between three positions: closed, clockwise and counterclockwise. A roller cam on the drive shaft engaged micro switches which were part of a mechanical relay logic chain. Two 24 volt control signals were used to select the desired valve position. While this system was extremely robust from a radiation
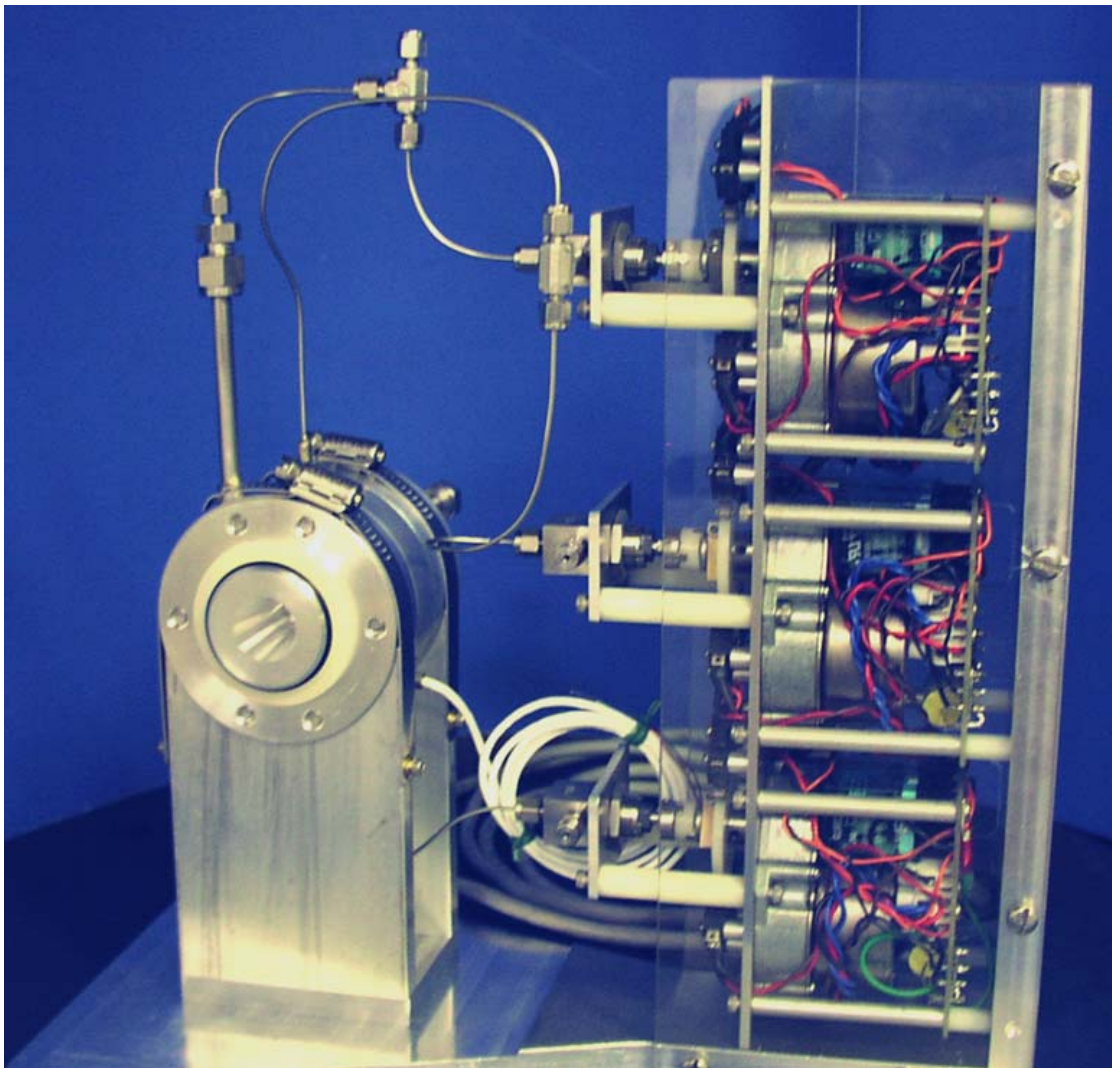
Figure 3-8: Version 1.0 Target and Target Filler

17

damage standpoint, it lacked reliability. The mechanism contained over 90 moving parts and seldom failed the same way twice. Ultimately, the only way to keep the system in service was to have complete replacement assemblies in inventory.

In contrast, the solenoid valves in the system were extremely reliable. The only drawback to these devices was the heat generated from continuous duty operation. Over time, the coil insulation would breakdown from heat fatigue. This would be addressed in the next system.

The pressure transducer was located in the base of the chamber flange. While this location provided an excellent measurement of internal pressure, the neutron flux in the vicinity of the beam strike dramatically shortened the effective service life of the piezoelectric sensor. After approximately one dozen irradiations, the transducer would need recalibration. After a dozen more, the transducer would have to be replaced.

The first system also suffered from unreliable product delivery. The helium supply provided three fixed pressures to move the liquid bolus. Low pressure would ease the volume from the target into the delivery line. Next, medium pressure would move the product through the line to the radiochemistry lab at a modest rate, as to not break the trailing end of the bolus. Finally, high pressure would produce a swift flow of helium to dry the delivery line. This worked well if the sequence was timed appropriately and the delivery line was relatively new. However, adjustments are often needed as the delivery line becomes radiation fatigued. This was a very tedious process which required mechanical adjustments at the helium supply system.

18

3.3 Control System 2.0

The second control system included a complete redesign of the target filler and helium supply system. These systems were intended to provide a research platform that could later be integrated into clinical production.

The majority of target filler components were mounted on a lexan backplane attached to the beam line mounting plate (Figure 3-9 and Figure 3-10). The entire target system can be removed from the beam line by disconnecting four fittings. This greatly simplifies maintenance and reduced dose since the bulk of the work can be done outside of the cyclotron vault. In addition, the backplane makes single component replacement much easier, as less disassembly of surrounding hardware is required.
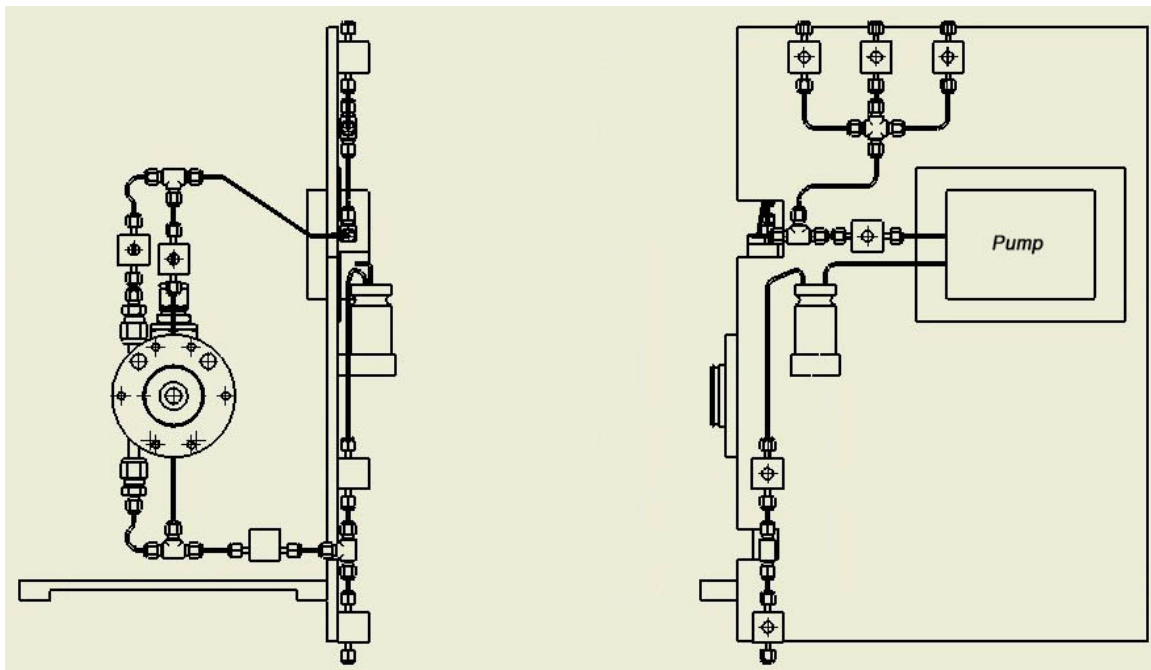
Figure 3-9: Version 2.0 Target and Target Filler Panel

19
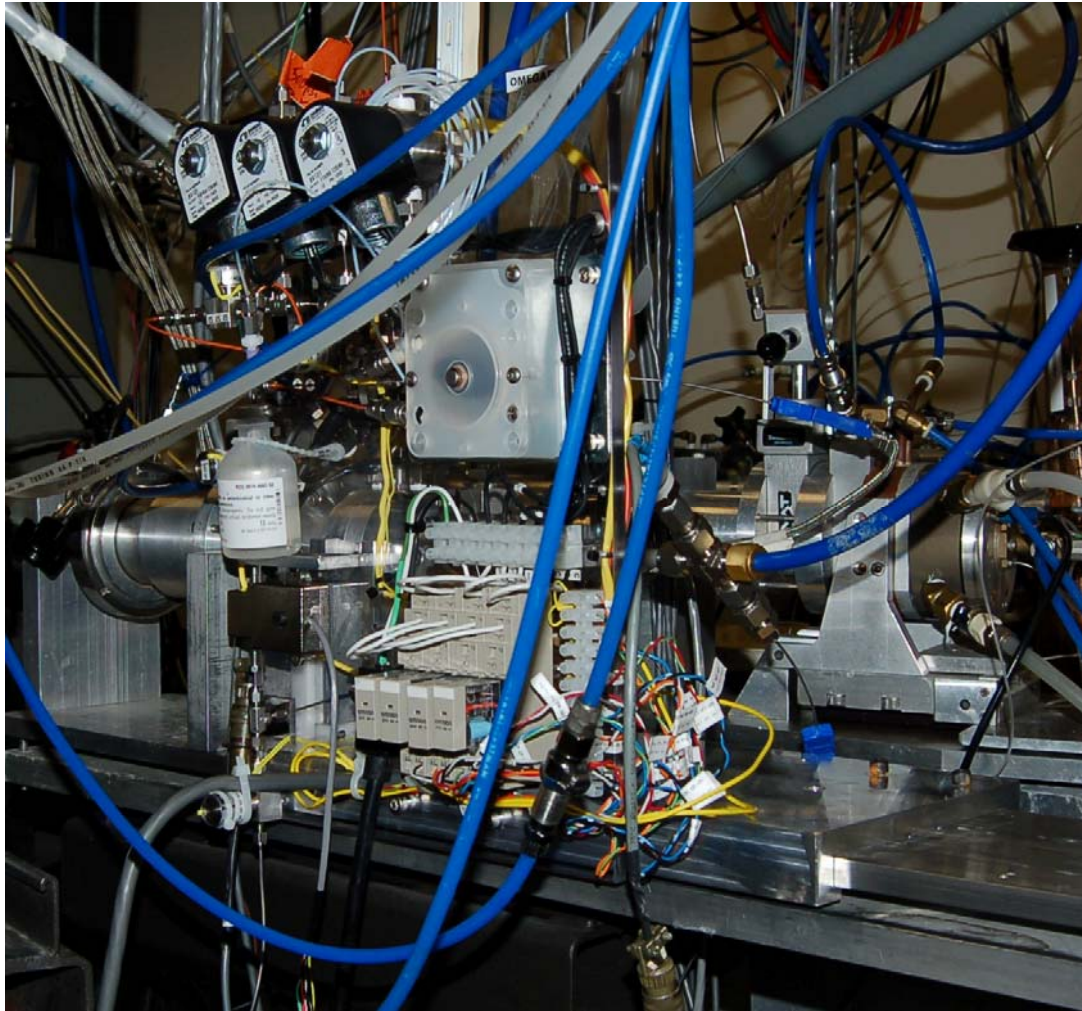
Figure 3-10: Version 2.0 Target and Filler Panel Installed on CS-30 Beam Line

The overall system reliability was improved tremendously by exclusively employing solenoid actuated valves. To resolve the issue of overheating, a CoolCube[TM][6] integrated circuit was added to each channel of the discrete output module. This device reduces the holding current for continuous duty operation so that the valve temperature does not rise significantly above room temperature.

20

An unamplified bonded foil pressure transducer was installed in the upper region of the expansion chamber. Due to the large dead volume of the transducer, it could not be used in the liquid region of the system. This design, though much less susceptible to radiation damage, did not provide a true measurement of internal target pressure due to damping effects. For the purposes of target control this was acceptable.

The helium supply system was improved by employing an eletropneumatic converter for low pressure control. This device generates a pressure output proportional to control voltage. The additional flexibility is very useful in the fine tuning of delivery sequences. The user interface is also much cleaner since fewer valves are used (Figure 3-11).
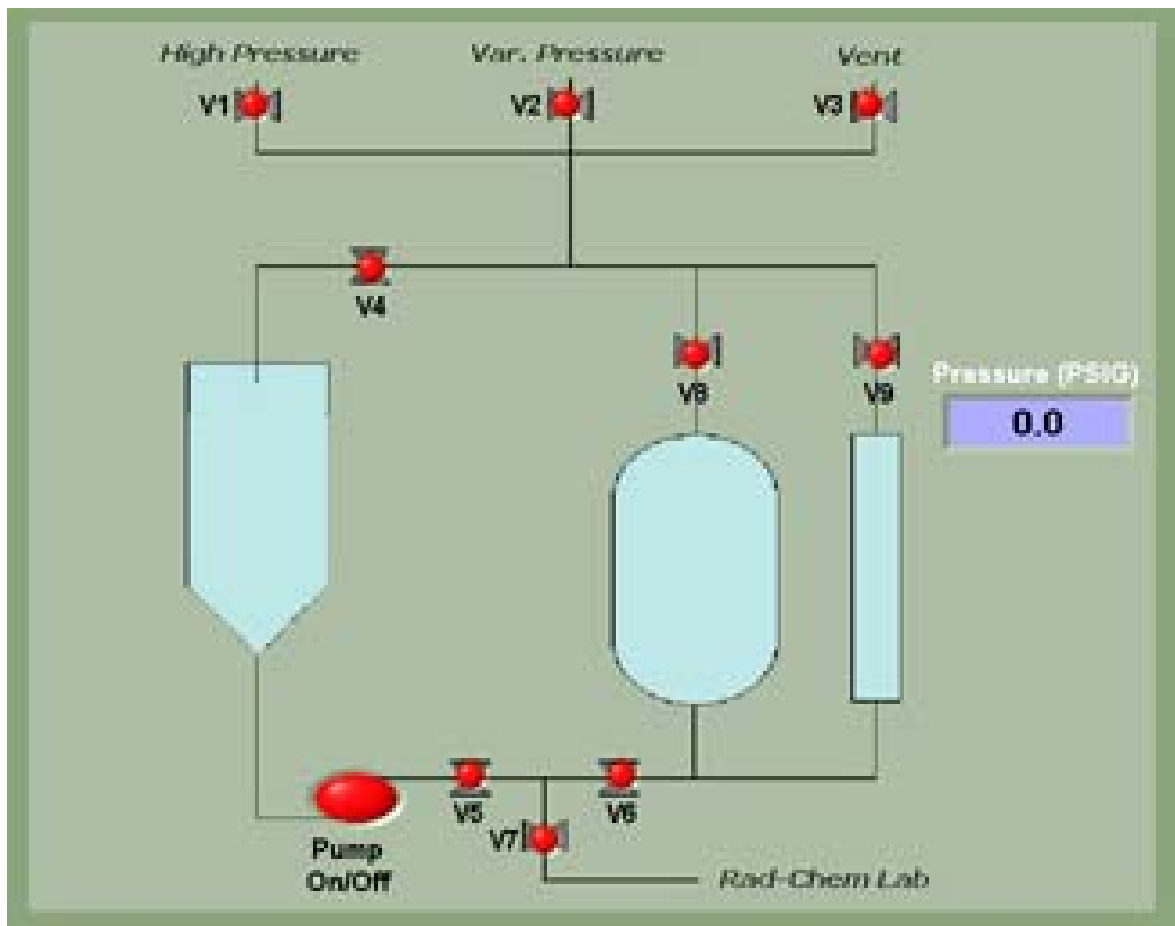
Figure 3-11: Version 2.0 Operator Interface

21

3.4 Control System 3.0

The third revision of the control system was driven primarily by the space limitations of the GE PETtrace. The target envelope is much smaller, specifically in the vertical dimension. For this reason, the expansion volume was relocated to the filler panel (Figure 3-12) which is located approximately two feet away. A lexan backplane was again utilized due to good performance in the previous system.

In order to conserve space, this system uses small solenoid driven diaphragm pumps to fill the target. These pumps fit easily onto the target filler panel. The dispensing accuracy is much lower than the previous metering pump, but this is acceptable due to the circulating flow path.

Target pressure was monitored with a zero dead volume flow through pressure transducer. This device combines the ruggedness of a bonded foil strain gauge with geometry suitable for use in the liquid region of the system. It is placed between the bottom target port and the expansion chamber so it provides an excellent reflection of internal pressure.

The helium supply system remained largely unchanged from the previous design. The WMC installation uses a higher capacity electropneumatic converter since the larger volume requires greater delivery pressure.

System 3.0 was first tested at the Duke PET facility, and later installed at WMC. This design has a very good, albeit relatively limited, track record. While the total number of irradiations performed is somewhat low, these systems have been installed in high radiation environments for longer than six months. Neither installation has required any component replacements to date.

22
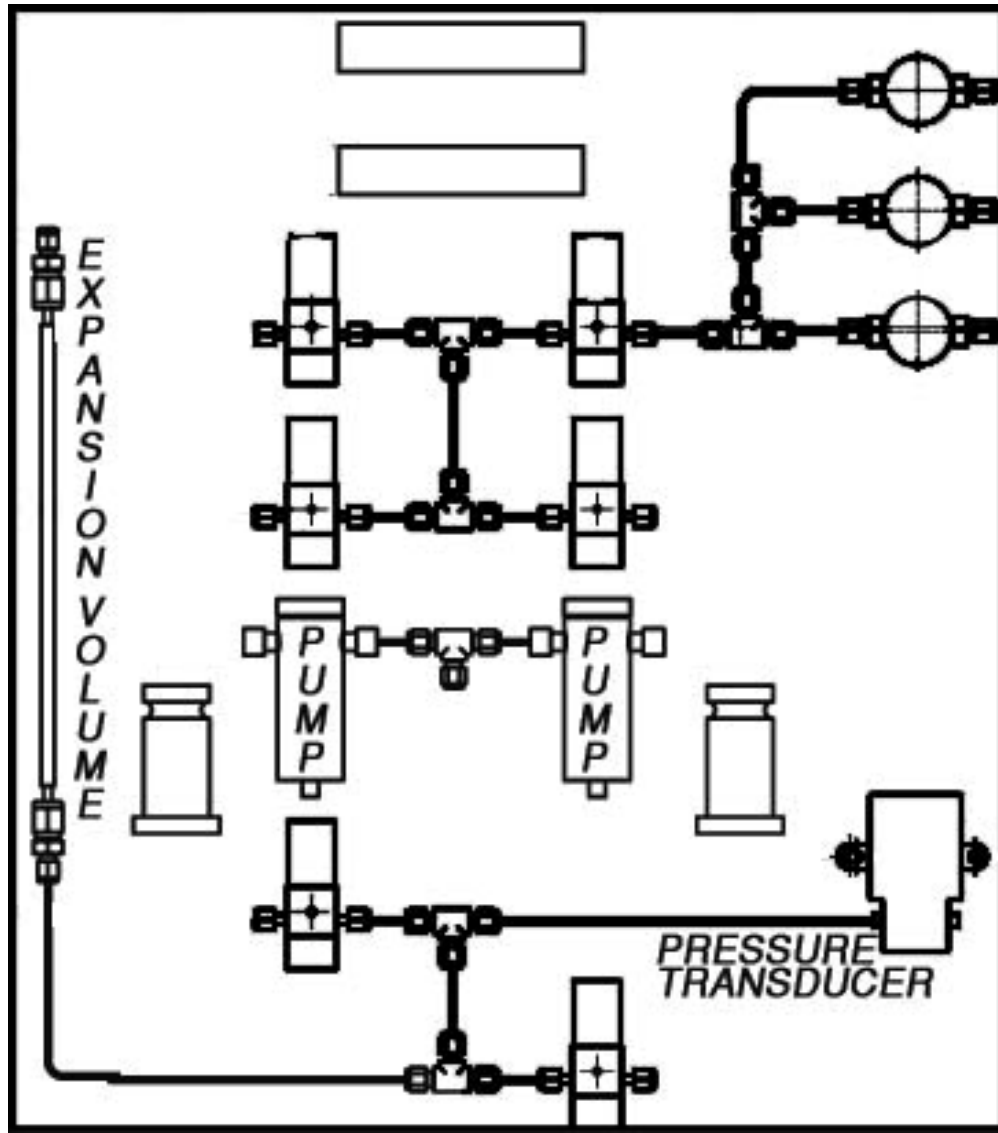
Figure 3-12: Version 3.0 Target Filler Panel

Since this control system is intended for research and production use, the software includes multiple modes. A manual mode is available for high level users to accommodate experiments and target maintenance. In the case of routine production, the software runs in an automated operator mode. The operator mode does not permit manual component-wise operation and forces the user to select from a list of preprogrammed sequences. These sequences may only be executed in a designated order to ensure proper operation.

23

Additionally, since no communication exists between the cyclotron and target controller, many warnings must be acknowledged by the operator during these sequences. These warnings will hopefully help manage failures due to operator error. The automated interface screen is included in Figure 3-13.
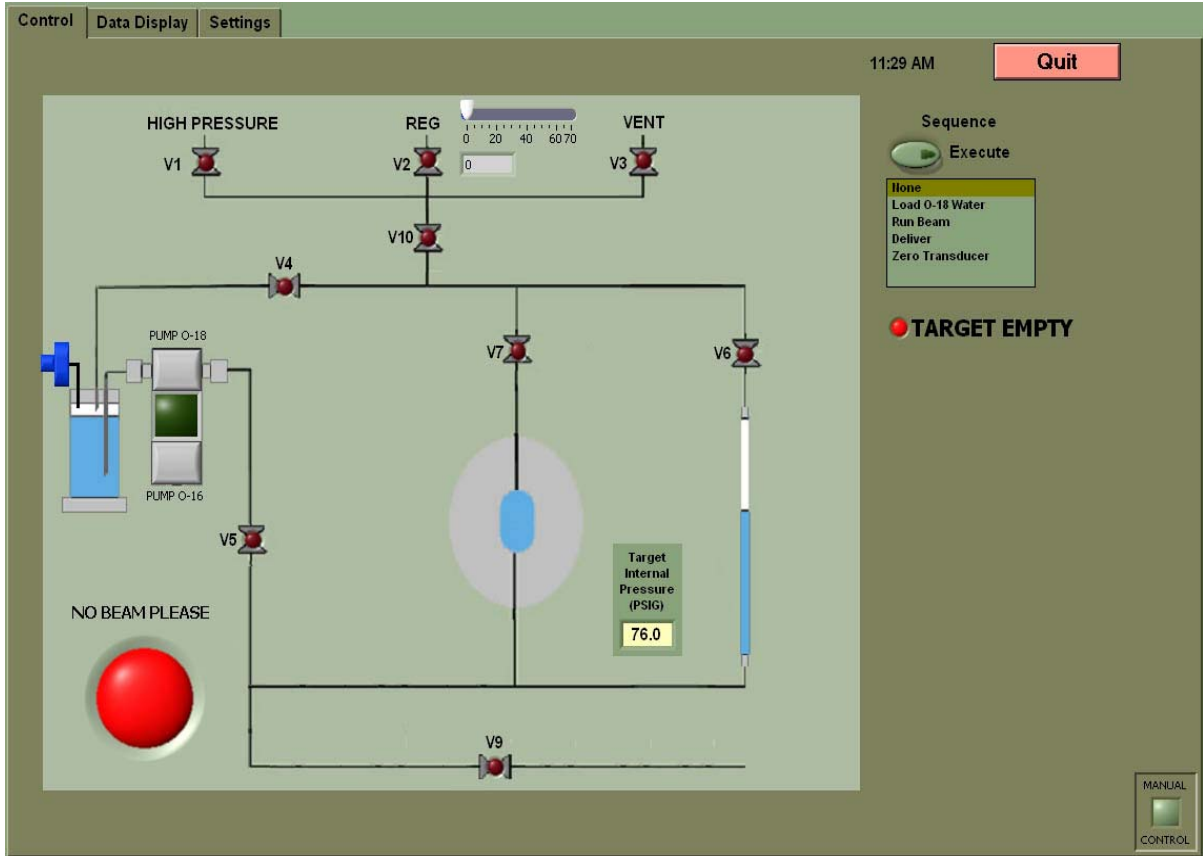
Figure 3-13: Version 3.0 Operator Interface

CHAPTER 4 - EXPERIMENTAL METHODS

4.1 Radiochemical Yield

The ultimate performance metric for an [O-18] water target is the amount of reactive [F-18]fluoride ion produced. Theoretical saturation yield values for the nuclear reactions of interest have been calculated using published cross section data [11,24].

Figure 4-1 shows liquid target saturation yields for ^{18}F and ^{13}N.
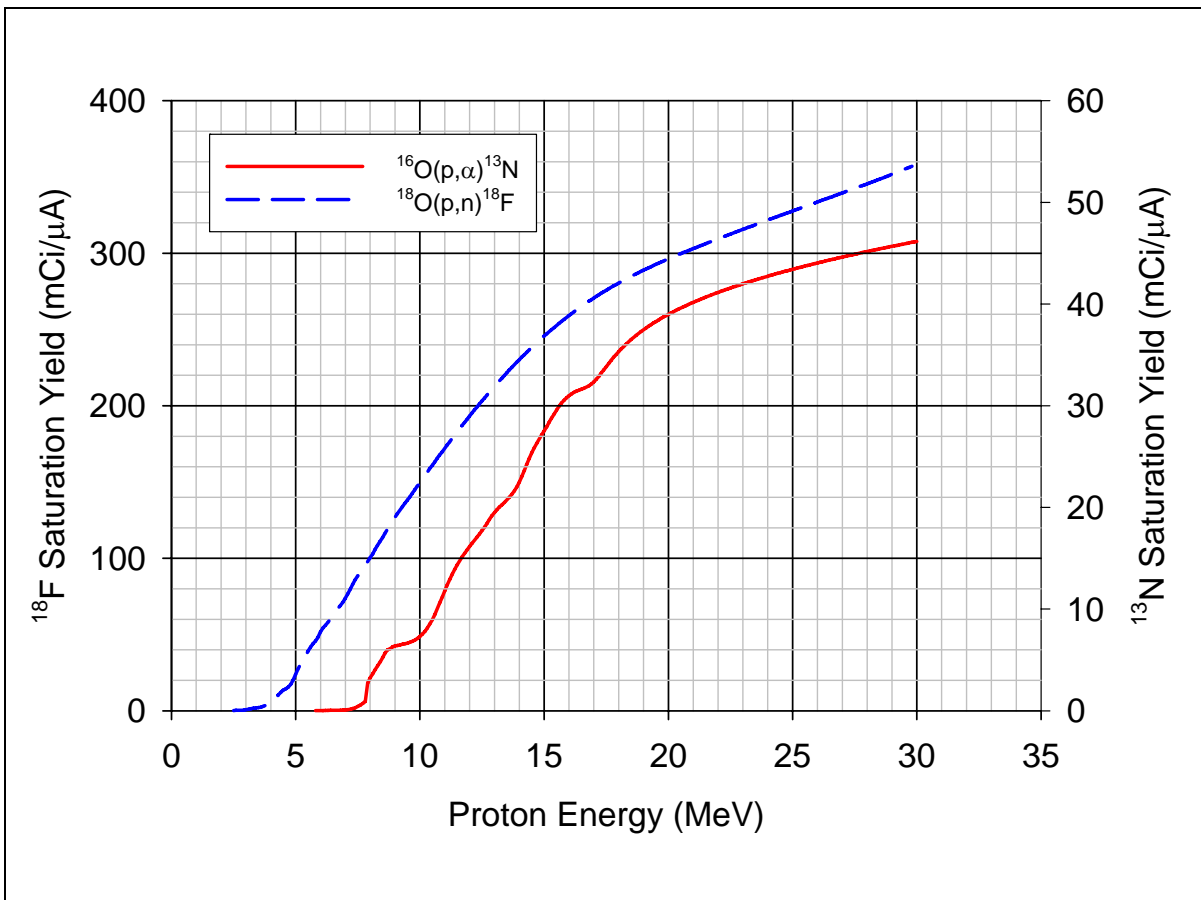
Figure 4-1: Theoretical Water Target Saturation Yields for ^{18}F and ^{13}N

Comparing the amount of activity produced in an irradiation to these theoretical values is an excellent indication of beam fluence in the target medium. Irradiations can be

performed using either natural abundance water or [^{18}O]enriched water. Natural abundance water offers the advantage of low cost, but the large amount of ^{16}O results in increased production of ^{13}N via ^{16}O(p,α)N^{13} for proton energies below 22 MeV and ^{15}O via ^{16}O(p,pn)^{15}O for proton energies above 16 MeV [20]. Enriched water is more costly, but results in a much larger fraction of ^{18}F$^-$ and simplifies analysis. Another advantage of enriched water is that the [^{18}F] fluoride activity can be synthesized into FDG, which gives an indication of the chemical quality of the product.

Finding the optimum intensity at which to run a target is accomplished by many irradiations on both natural abundance and enriched material. This is an expensive and time consuming process. While it yields critical information, it does not provide a complete picture of the physical processes in the target. For this reason, it is important to measure other physical parameters.

4.2 Sight Tube Analysis

Vapor fraction in the beam strike is the most critical parameter concerning target penetration. Though the local vapor fraction in the proton beam cannot be measured directly, the target averaged vapor fraction can be measured by means of a glass sight tube. The sight tube is attached between the expansion chamber and helium supply valve and has an internal diameter and length appropriate for the target fill volume. The target is filled until water is visible in the sight tube, pressurized, and irradiated. An illustration of the sight tube before and during irradiation is included in Figure 4-2.

26
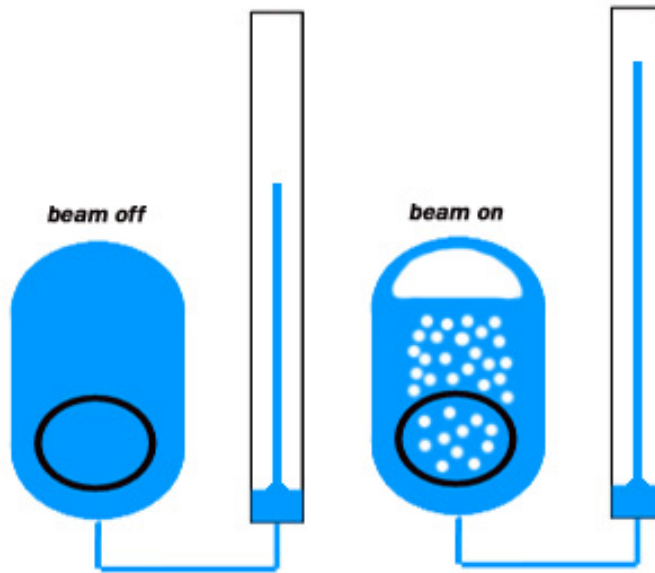
Figure 4-2: Sight Tube Connected Above Expansion Volume

The regions of operation can be observed by inspecting the sight tube level as a function of beam current. The operating modes are listed below:

1. Single Phase Convection – linear rise in level from thermal expansion
2. Subcooled Window Boiling – minute erratic level movement
3. Subcooled In-Beam Boiling – small level oscillations
4. Bulk In-Beam Boiling – regular level oscillations with magnitude proportional to beam intensity
5. Thermosyphon Boiling – displaced volume very insensitive to increases in power with small deviation from mean level
6. Penetration (controlled) – maximum level plateaus while minimum level continues to rise
7. Penetration (severe) – violent swings in level (frequency and displacement)

27

Each of these modes corresponds to a specific time dependent behavior of the internal target pressure. This can be observed by installing a pressure transducer between the chamber and expansion volume. Analysis of the boiling kinetics has been reserved for future work. It should be noted that true thermosyphon boiling has yet to be observed in any target, presumably due to the small chamber dimensions. Controlled penetration has been seen in targets tested at WMC, while the Duke targets transitioned directly from bulk boiling to severe penetration. These experiments will be discussed further in the research summary.

Penetration results from insufficient target mass along the proton track. Charged particle transport is well understood and proton ranges can be calculated for a variety of compounds, energies and geometries. Range thickness values have been calculated for volume averaged two phase distributions (Figure 4-3).

Minimum Target Thickness for Void Fraction (Density) Limit
400 psig Saturation Conditions
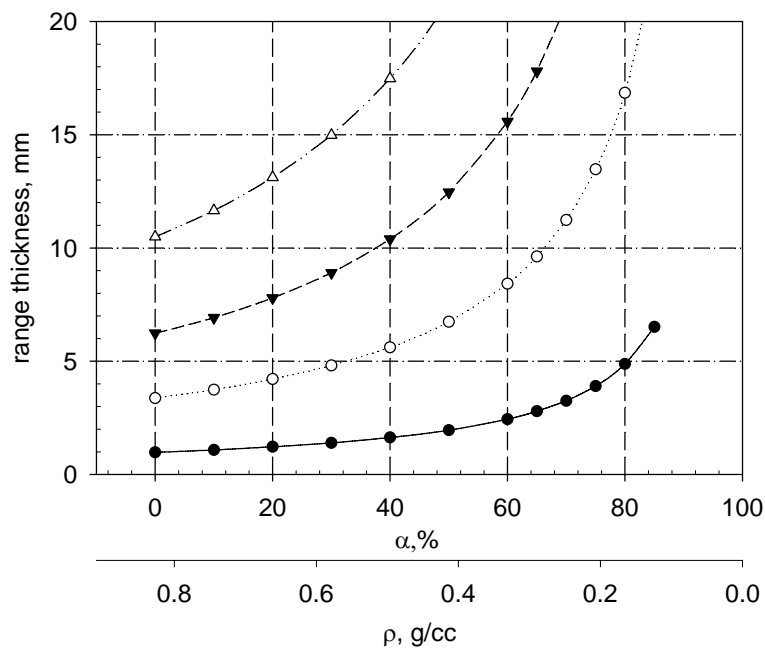
Figure 4-3: Range Thickness as a Function of Average Void Fraction

28

The uncertainty in range thickness for a boiling target results from the distribution of liquid and vapor in the beam path. For any target operating at steady state, there exists a slight imbalance between the vapor generation and condensation rates. This is the product of small system volume and a volumetric heat input that is spatially dense. The imbalance is evident by the oscillations in the sight tube level. Phenomenological models can accurately predict heat transfer using a time-averaged value of target void fraction. However, the effective proton range is significantly less than would be expected for this average value due to variations in beam strike void. Determining the appropriate design margin for target depth is a high priority task for computational efforts in this area.

4.3 Flow and Calorimetric Analysis

Pressure versus flow measurements were taken for four of the six experimental targets. These data were used primarily for calculating heat transfer coefficients in computational models. Additionally, in some cases, inlet and exit temperatures were also measured and total heat transfer from the target by cooling water was directly measured.

CHAPTER 5 - EXPERIMENTAL TARGET SYSTEMS

5.1 Previous Thermosyphon Targets

Three generations of experimental thermosyphon target systems were developed prior to this work [19]. The purpose of these targets was to determine the feasibility of bottom pressurized operation and initiate experimental and computational platforms for target design and analysis. These targets had relatively simple geometries and were not intended for clinical production.

5.2 Fourth Generation Thermosyphon Targets

5.2.1 TS4-DUKE

The fourth thermosyphon design was intended for target research at the Duke CS-30. It had a monolithic silver body with a chamber diameter of 10 mm and depth of 15 mm. The TS4 designs had a relatively large conduction distance from the chamber wall to the radial cooling channels. This was due to the manifold geometry resulting from the seals on the target window (Figure 5-1). The penalty for this conduction distance may not have been realized initially but would prove significant in future tantalum designs [24].

The maximum beam current that can be extracted via the deflector and magnetic channel is approximately 45 µA (1170 W at full energy). Sight tube experiments conducted on this target indicated that at this beam current, the target had not reached its thermal limit (Figure 5-2). Enriched water yields were conducted up to 35 µA (910 W), which was expected to be the maximum beam current for production.

30
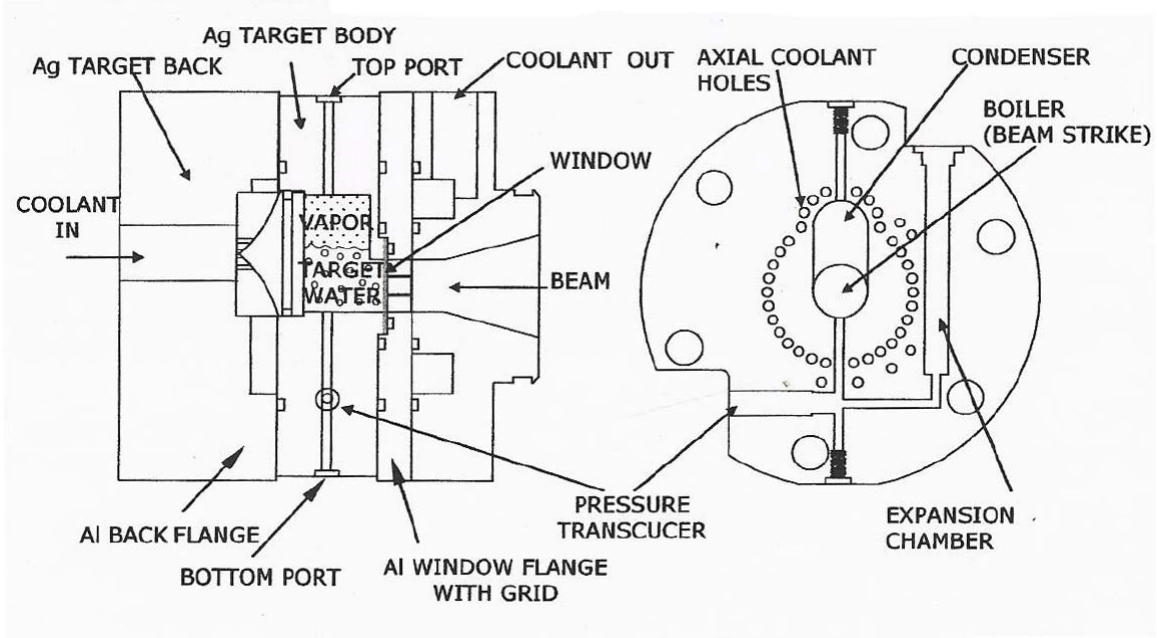
Figure 5-1: TS4-DUKE Target Chamber Flange

TS4-DUKE 26 Mev 400 psig
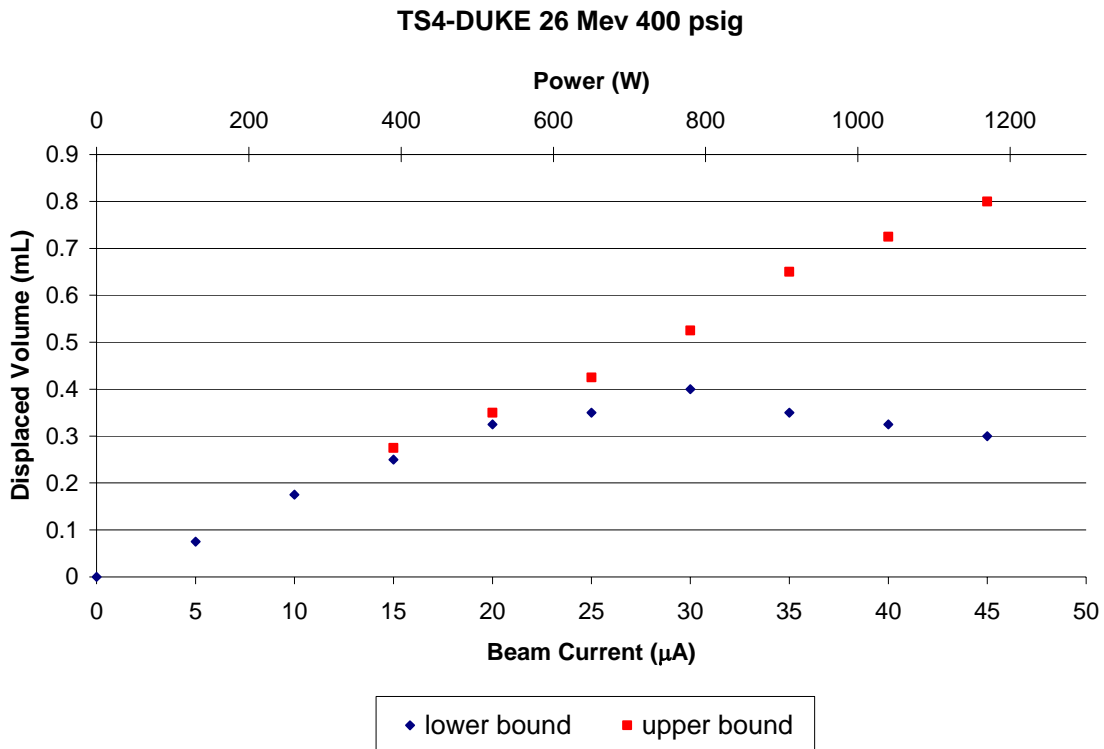
Figure 5-2: TS4-DUKE Sight Tube Results

31

While the yields of $^{18}F^-$ were adequate (85-95% of theoretical), the uncorrected post-synthesis ^{18}FDG yield from the TracerLab MX unit was consistently below 50 percent. To investigate this further, an irradiated water sample from the thermosyphon was manually delivered through the ion exchange resin, followed by a sample from the production target. The low FDG yield persisted, indicating potential contamination rather than a $^{18}F^-$ reactivity issue.

There was initially little information regarding high intensity irradiations using silver target bodies since most target designers have adopted tantalum or niobium. Recent target experiments have shown good performance with silver chambers at elevated power levels with negative ion cyclotrons. It is likely that limited localized target penetration due to the very tight beam aggravated the target chemistry. This would not be evident from sight tube experiments if significant penetration of the fluid bulk did not occur.

5.2.2 TS4-CYC30

Establishing a research agreement with a large pharmaceutical manufacturer resulted in beam time on an IBA Cyclone-30. This was a unique opportunity due to the high current output of the cyclotron. The test target was a scaled up version of the TS4-DUKE target, intended to accommodate the larger 15 mm beam. The target body construction was monolithic silver, and had a grid supported Havar window. Sight tube measurements were recorded for currents up to 125 μA at a proton energy of 26 MeV (3250 W). No measurable oscillation in the liquid level was observed. The displaced volume increased monotonically with beam current and showed no indication of beam penetration (Figure 5-3).

32

TS4-CYC30 26 Mev 400 psig
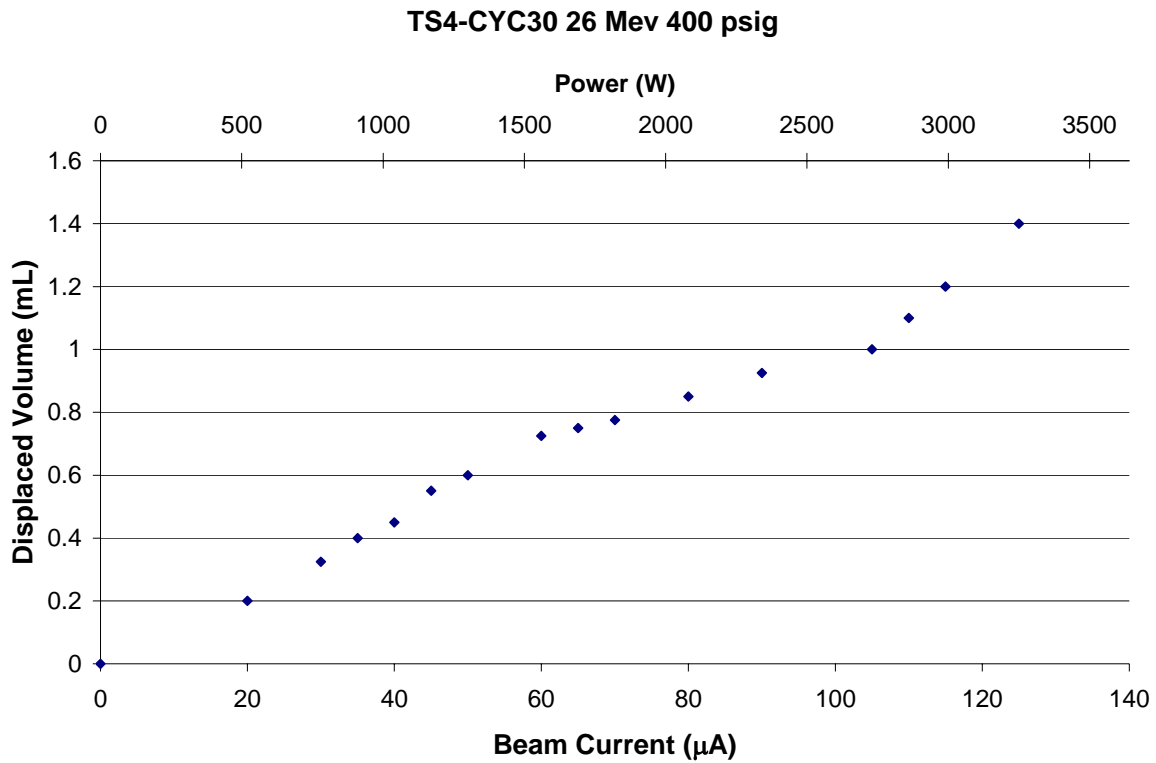
Figure 5-3: TS4-CYC30 Sight Tube Results

Initial attempts to perform natural abundance water yields were impeded due to the combination of positive vault pressure and $^{13}N_2$ escaping the target during depressurization. Without proper exhaust in the target vault, $^{13}N_2$ entered personnel areas and triggered area radiation alarms. Irradiations were halted until vault maintenance was completed several months later. Unfortunately, due to a fault in the cooling water system, the target suffered a catastrophic failure during the next irradiation.

Attempts were made to remanufacture the target utilizing the intact components, but the relationship with the facility dissolved before any more meaningful data could be recorded. The target system remains in radioactive material storage at the site. The thermal limit has not yet been determined.

33

5.3 Fifth Generation Thermosyphon

The characterization and analysis of this target has been documented in previous work [15,24]. The target had an internal volume of 1.3 cc and a depth of 10 mm. While it was useful for developing analysis techniques, it was ill-suited for production. It should be noted that the radial cooling channels were located outside the outer window o-ring (Figure 5-4).
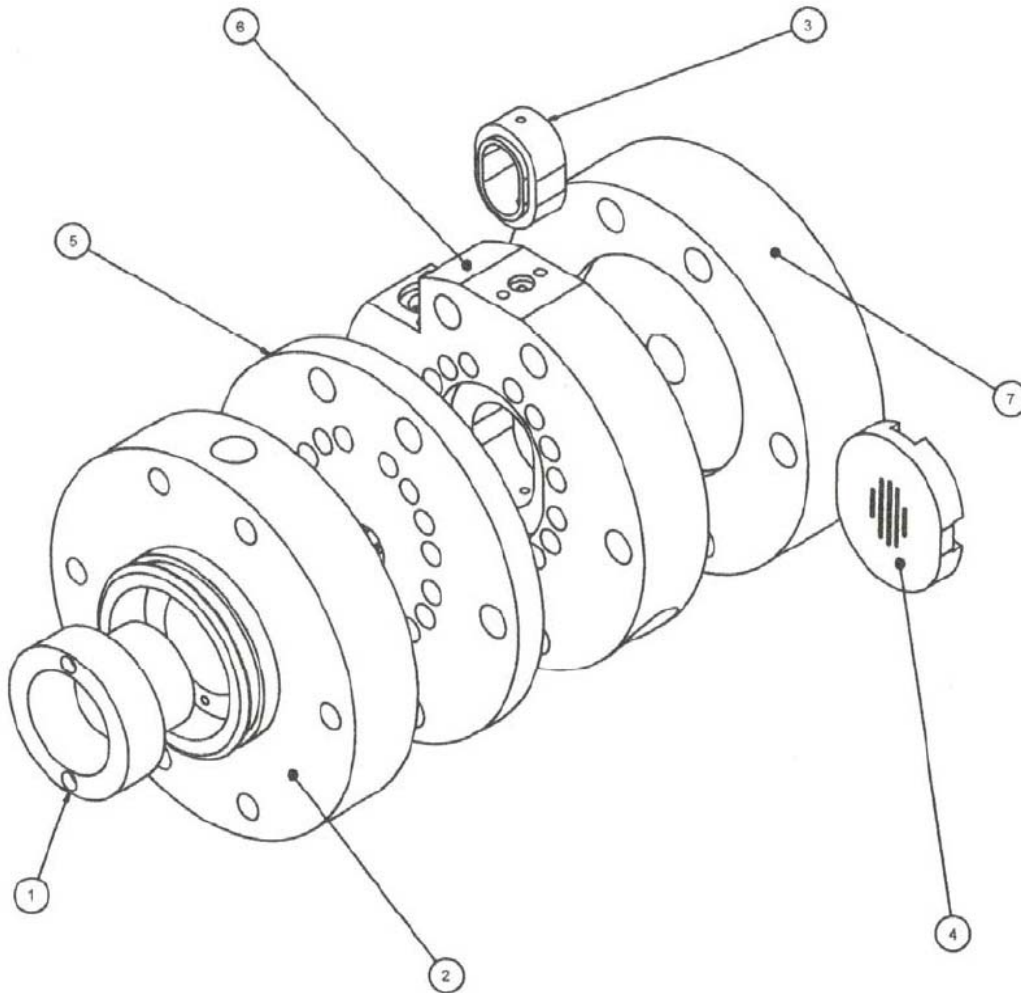
Figure 5-4: TS5 Exploded Parts Diagram (Humphrey 2006)

CHAPTER 6 - PRODUCTION TARGET SYSTEMS

6.1 TS6-DUKE

The TS6-DUKE system had two design objectives. The primary objective was to collect data for validating computational models. Additionally, Duke was provided with a tantalum production target. The target body is constructed of aluminum and houses a tantalum insert containing the chamber. All wetted parts are tantalum or 300 series stainless steel. The chamber has an internal volume of 1.9 cc, which corresponds to enriched water consumption per irradiation of approximately 2.3 cc. This target was the first to incorporate a target insert geometry in which the radial channels could be located closer than the distance from the chamber wall to the inside window o-ring (Figure 6-1 and Figure 6-2).
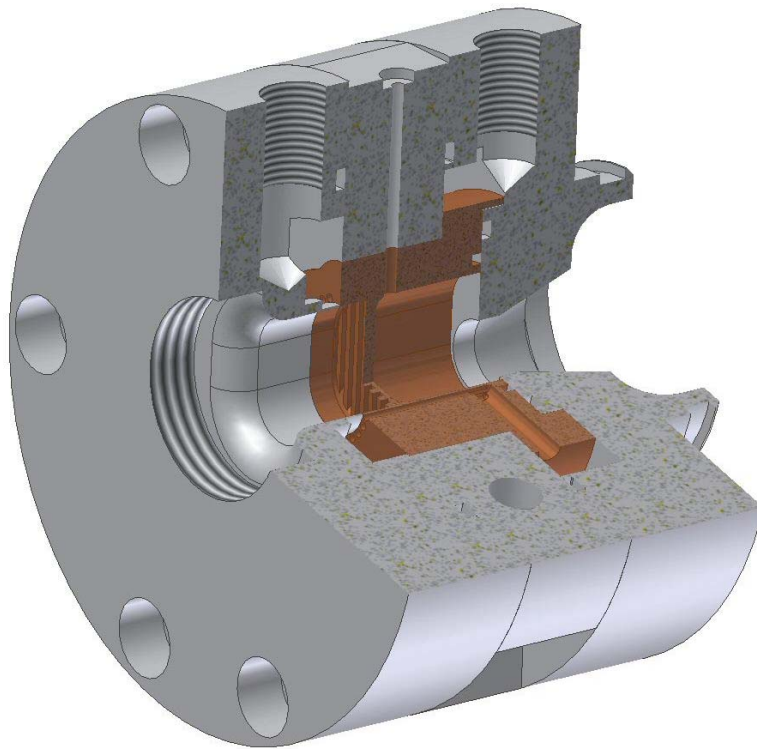
Figure 6-1: TS6 Assembled Solid Model (Humphrey 2006)
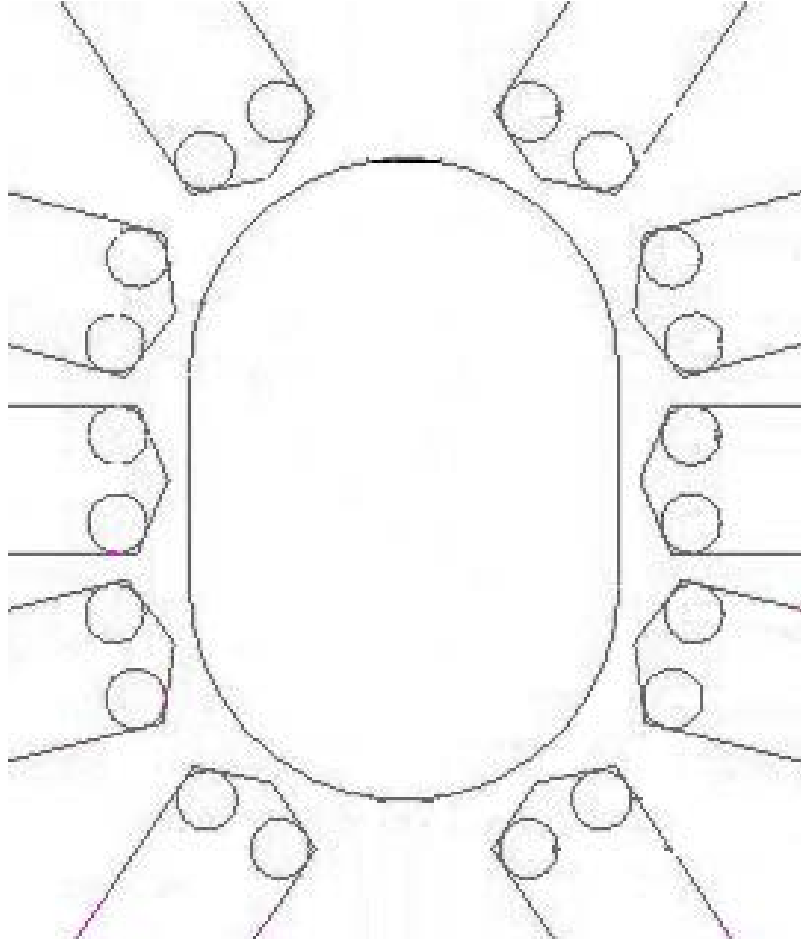
Figure 6-2: Cross Section of TS6-DUKE Target Insert

6.1.1 Cooling Flow and Calorimetric Characterization

The TS6 was designed primarily as a modeling tool and has features tailored to observing heat transfer behavior during irradiation. The radial and axial cooling water circuits are isolated so that temperature rise and flow rate can be measured online to estimate heat transfer in each loop separately. The overall forms loss coefficients were determined by recording the mass flow rate in each cooling circuit as a function of pressure drop. Flow was first measured in the laboratory using a Rosemount 1151 mass flow meter, while differential pressure was measured across the target using an Omegadyne PX51-100. This model

36

differential pressure transducer employs a bonded foil strain element in a full bridge configuration with no output amplification, making it very tolerant to radiation dose. Using the experimentally determined forms loss coefficients, flow could be monitored in the cyclotron vault by measuring differential pressure across the target. Fitted curves for each cooling circuit are shown in Figure 6-3.

TS6 Flow vs. Pressure Drop
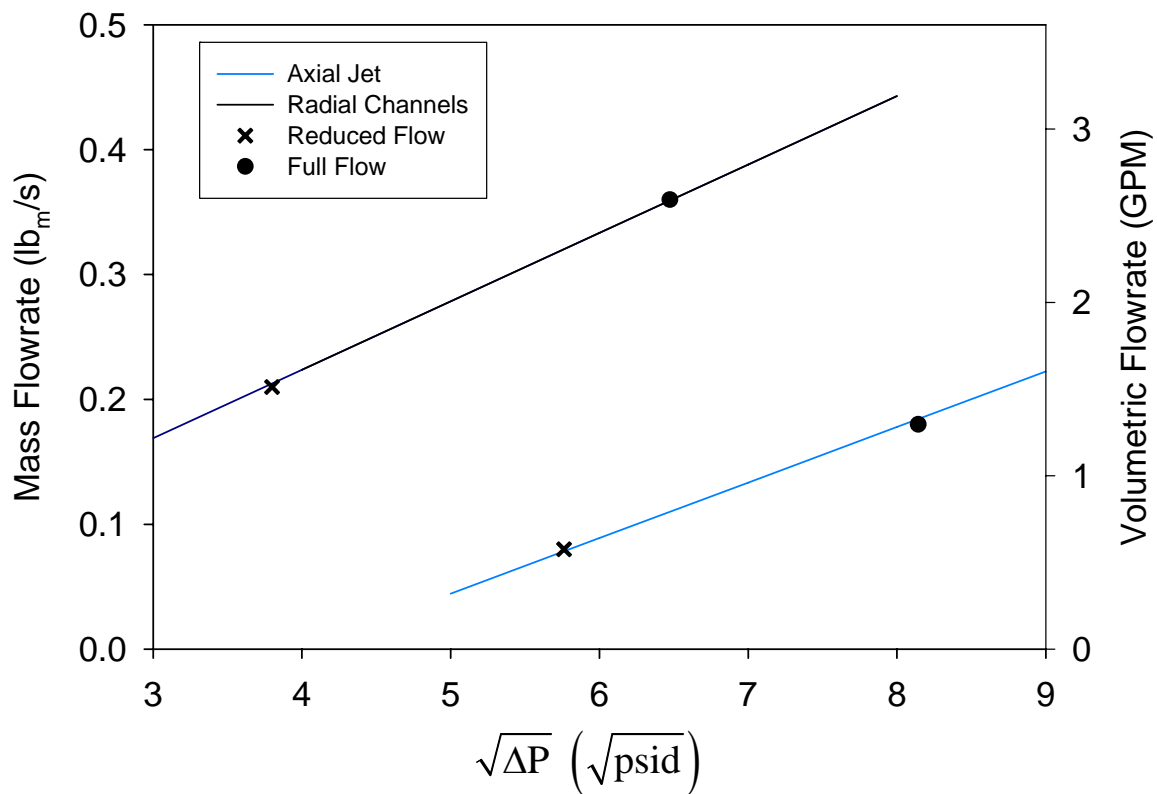
Figure 6-3: TS6-DUKE Cooling Flow Characterization

Inlet and outlet cooling water temperatures were measured during irradiation using type T thermocouples to calculate the heat removal in each cooling circuit. Under full manifold pressure, the temperature rise was too small to measure with confidence and the

37

cooling flow had to be substantially reduced. This was achieved by installing manual ball valves in the cooling water supply lines.

Beam current was measured electronically by installing a buffered differential amplifier across the auxiliary output of the beam current integrator at the cyclotron control panel. The thermal power measured in the cooling water was within 5% of the beam power for the range of incident beam currents. This provides information about how the heat transfer is distributed as well as verifying the magnitude of heat input with an additional measurement. The calorimetric data are included in Figure 6-4.
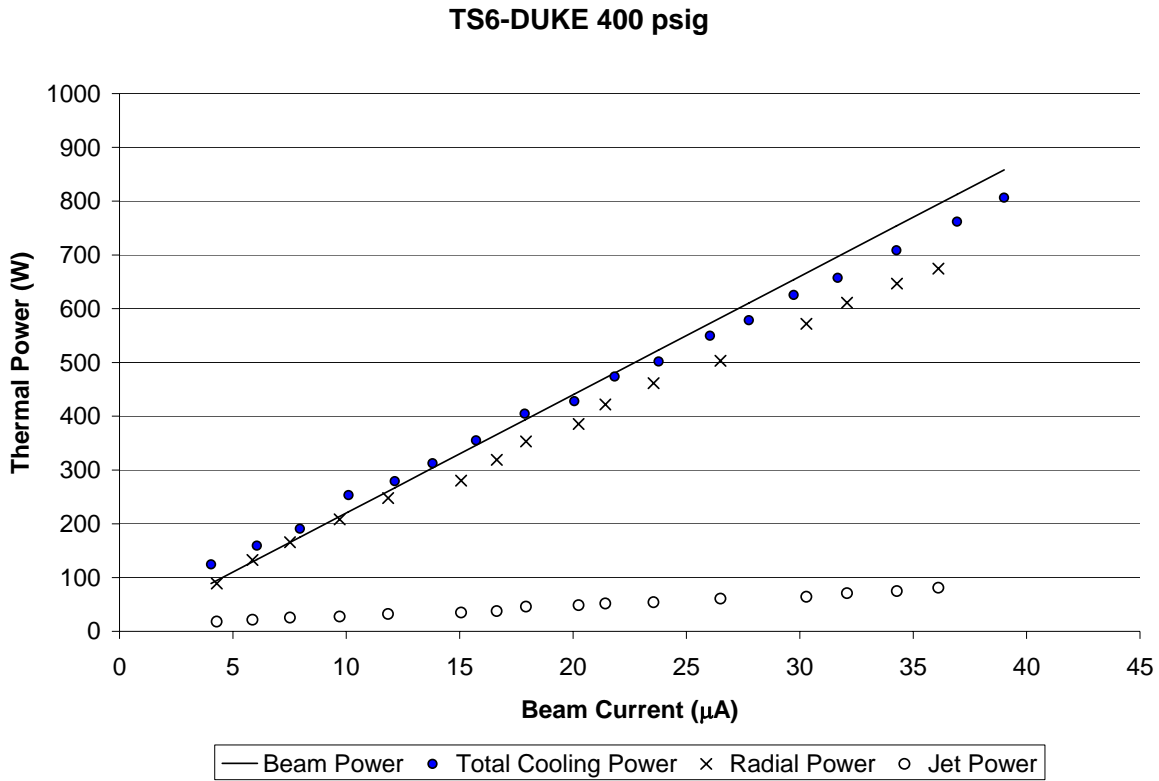
TS6-DUKE 400 psig

Figure 6-4: TS6-DUKE Calorimetric Data

38

6.1.2 Sight Tube Analysis

The first set of sight tube data was collected at a beam energy of 22 MeV, full cooling flow and an overpressure of 400 psig. These would be the typical parameters for daily production. Under these conditions, the target does not exhibit behavior indicative of penetration at beam currents up to 40 µA (880 W), the maximum output available for the CS-30 at the time. Sight tube measurements are included in Figure 6-5.

TS6-DUKE 22 MeV, 400 psig, Maximum Cooling Flow
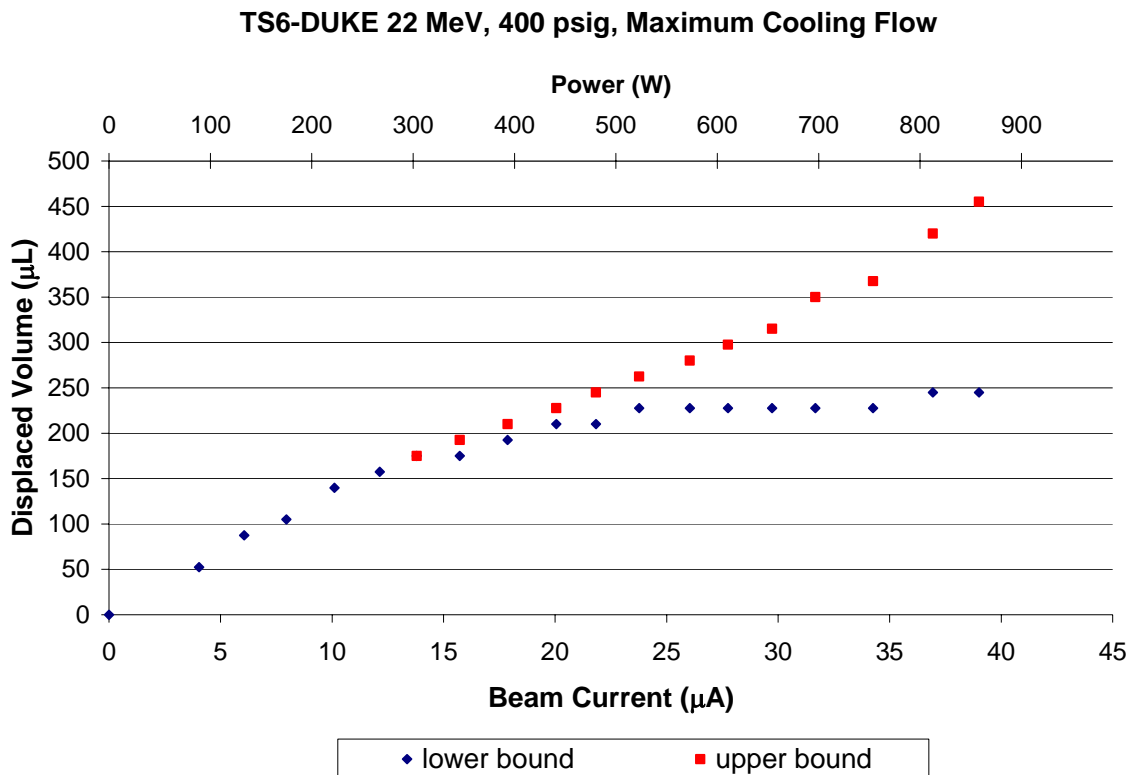
Figure 6-5: Sight Tube Data for Normal Operating Parameters

These data suggest that the target is operating in a bulk boiling mode above approximately 22 µA. The maximum displaced volume increases with intensity but in a steady, controlled fashion. Without the capacity to run at higher beam current, the ultimate performance limit cannot be determined. However, operation up to 1 kW appears reasonable.

39

While this is an excellent result from a production standpoint, the behavior at the target thermal limit is also of interest for model validation. In order to observe these behaviors, penetration of the target can be achieved by perturbing selected operating parameters. Decreasing the overpressure or reducing the cooling flow rate reduces the effective heat rejection capacity of the system and leads to penetration at lower beam currents. Figure 6-6 includes sight tube data for the reduced cooling flow rates shown earlier.

Sight Tube Data for 22 Mev, Reduced Cooling Flow, 400 psig
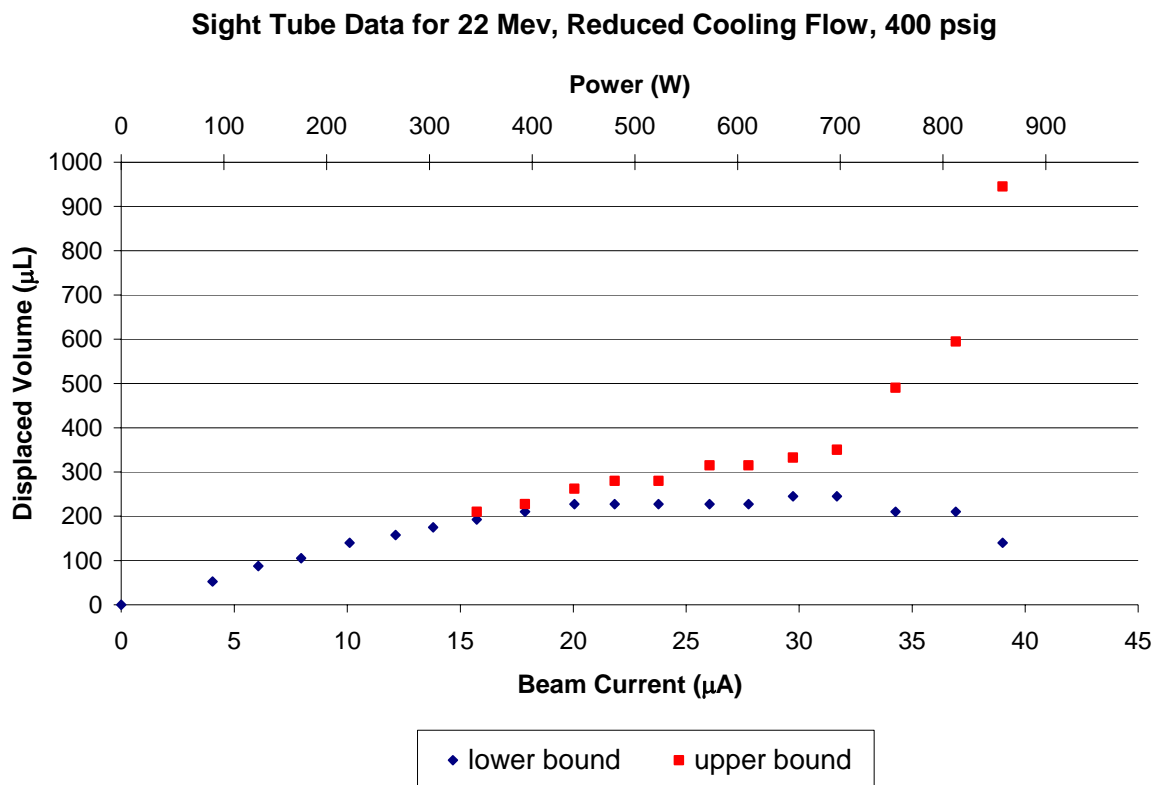
Figure 6-6: Sight Tube Data for Reduced Cooling Flow

Due to the reduced cooling flow, the convective heat transfer coefficients on the exterior cooling surfaces are degraded. This condition forces the chamber surface temperature to increase in order to transfer the same amount of power and ultimately leads to a rise in target void fraction. The sight tube behavior above 35 µA is indicative of target

40

penetration. The upper bound for displaced liquid rises dramatically while the lower bound drops. This is a transient behavior resulting from an imbalance of heat input and removal in the target liquid. As the target is sufficiently voided, the effective range thickness is less than what is required to completely stop the beam. Beam power is then deposited into the solid material of the target back, causing the voids to collapse. Above the thermal limit, this process repeats indefinitely at a frequency that increases with additional heat input.

The thermal limit of the target is also very sensitive to the magnitude of the helium overpressure. As the overpressure is decreased, the specific volume of the water vapor increases dramatically. As a result, the void fraction for a given energy content is much greater. This is aggravated by the small dimensions of the target chamber. The bubble dimensions are likely close in size to the target chamber, which can create flow stagnation or "vapor lock". This is evident from the sharp transition from bulk boiling to penetration when compared to the reduced flow case. Figure 6-7 includes the sight tube data at an overpressure of 100 psig.

6.1.3 Radiochemical Yield Data

Enriched and natural abundance water yield experiments were conducted at power levels suitable for production with good results. Due to the depth of the chamber, it is difficult to get a complete recovery of the water in the chamber without performing a rinse. Fluorine-18 yields ranging from 75 to 85% are common without rinse. A taper was added to future chambers to avoid this issue. The target body seals were also redesigned.

41

TS6-DUKE 22 MeV, 100 psig, Maximum Cooling Flow
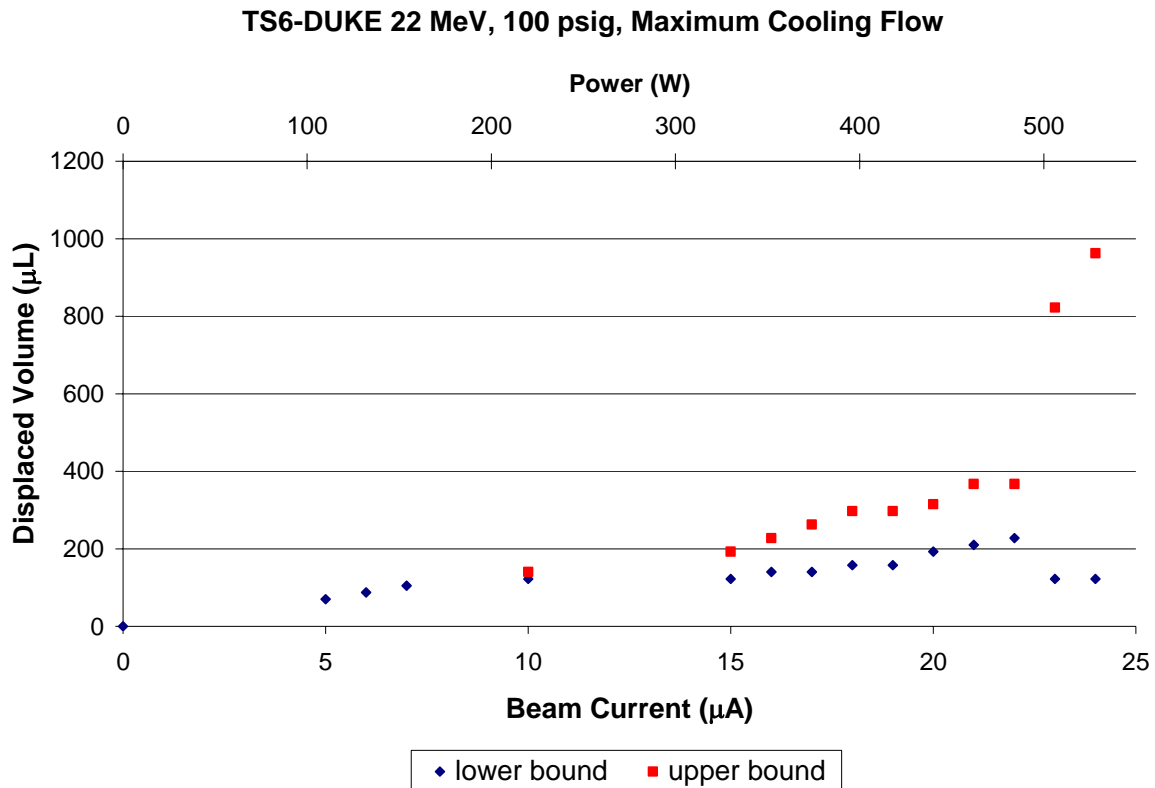
Figure 6-7: Sight Tube Data for Reduced System Pressure

Since the thermal characterization of the TS6 target system, power supply and vacuum related issues have degraded the performance of the CS-30 cyclotron. The current limit for extracted beam is approximately 35 μA. Due to this fact, the aluminum degrader was removed from the target collimator assembly increasing the beam energy to approximately 26 MeV. Doing so provided a marginal increase in yield to offset the reduced current capability without challenging the target.

6.1.3.1 $^{16}O(p,\alpha)^{13}N$ Yield Data

A summary of natural abundance irradiations are included in Figure 6-8 and Table 6-1. The theoretical saturation yield according to IAEA Nuclear Data Service is included for

42

TS6 ^{13}N Yield Data 26 MeV
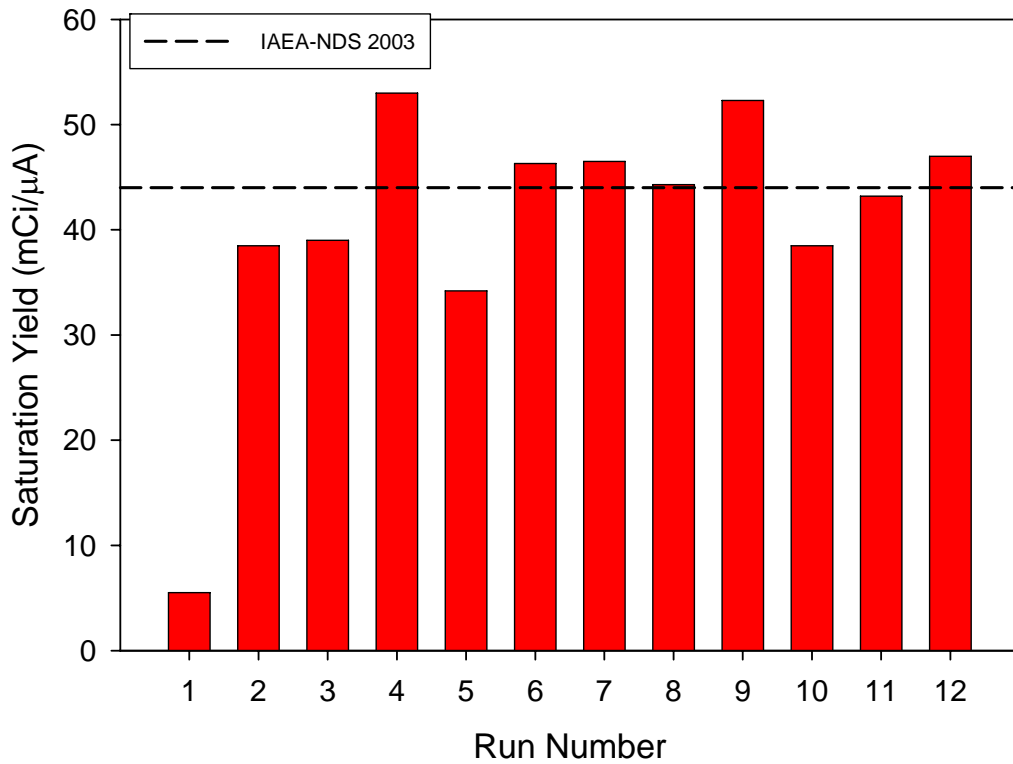
Figure 6-8: Summary of ^{13}N Yield Data

Table 6-1: Summary of ^{13}N Yield Data

Run	Date	Nuclear Reaction	I_{beam} (μA)	t (min.)	TTY (mCi/μA)
1	9/17/2007	$^{16}O(p,\alpha)^{13}N$	25	30	5.5
2	9/18/2007	$^{16}O(p,\alpha)^{13}N$	10	10	38.5
3	9/18/2007	$^{16}O(p,\alpha)^{13}N$	10	10	39.0
4	9/18/2007	$^{16}O(p,\alpha)^{13}N$	20	11	53.0
5	11/21/2007	$^{16}O(p,\alpha)^{13}N$	15	11	34.2
6	11/21/2007	$^{16}O(p,\alpha)^{13}N$	20	11	46.3
7	11/21/2007	$^{16}O(p,\alpha)^{13}N$	25	10	46.5
8	11/21/2007	$^{16}O(p,\alpha)^{13}N$	30	10	44.3
9	11/26/2007	$^{16}O(p,\alpha)^{13}N$	20	10	52.3
10	11/26/2007	$^{16}O(p,\alpha)^{13}N$	20	10	38.5
11	11/26/2007	$^{16}O(p,\alpha)^{13}N$	20	10	43.2
12	11/26/2007	$^{16}O(p,\alpha)^{13}N$	20	10	47.0

comparison[11].These irradiations were performed at 26 MeV using a 200 ppm ethanol in natural abundance water mixture to mitigate the production of $^{13}N_2$[27]. There is a significant amount of $H_2^{15}O$ produced at this energy from the $^{16}O(p,pn)^{15}O$ nuclear reaction. To determine the physical yield of ^{13}N at end of bombardment (EOB), the decay data was fitted using nonlinear regression in SigmaPlot [22]. Saturation yield was then calculated from the activity at EOB.

6.1.3.2 $^{18}O(p,n)^{18}F$ Yield Data

The following irradiations were performed at 26 MeV using [O-18]enriched water. Contamination issues from corrosion in the sight tube material initially resulted in low yields (~25%). Assaying a swab of the material shortly after irradiation revealed a large component of trapped [F-18]fluoride ion. After a thorough ultrasonic cleaning of the system, the performance dramatically increased. A small fraction of activity is still unrecoverable without a target rinse. A summary of enriched water irradiations are included in Figure 6-9 and Table 6-2.

6.1.4 Target Qualification and Clinical Production

The qualification of a production target at most radio pharmacies typically includes three test irradiations. These test batches are synthesized into ^{18}FDG and standard quality control (QC) checks are performed. These include but are not limited to pH, half-life, Thin Layer Chromatography (TLC), pyrogenicity, and sterility. Upon successful completion of these tests, the target can be used for clinical fluoride production.

The existing Duke production system consists of a low pressure reflux target,

44

operated at a maximum beam intensity of 20 µA at an energy of 18 MeV. This target initially consumes approximately 1.5 mL of enriched water per irradiation but must be partially refilled after 1 hour due to radiolysis. The TS6 offers significant performance gains in contrast to this system both from a standpoint of fluoride production and operational robustness.

The TS6 system has been successfully qualified for clinical production at the Duke PET facility. Unfortunately, cyclotron operations have ceased indefinitely due to construction of additional PET/CT scanner rooms and delivery line shielding. Upon completion of these tasks, production data will be available from the target system.

A set of production curves are included in Figure 6-10. These calculations assume a conservative saturation yield of 280 mCi/µA. The implementation of this target system will both increase the total production capacity of the site and add operational flexibility. This is very important with the addition of new scanners and an increased patient load. Producing clinical doses in less time also creates production space for experimental processes and compounds used for research.

45

TS6 ^{18}F Yield Data 26 MeV
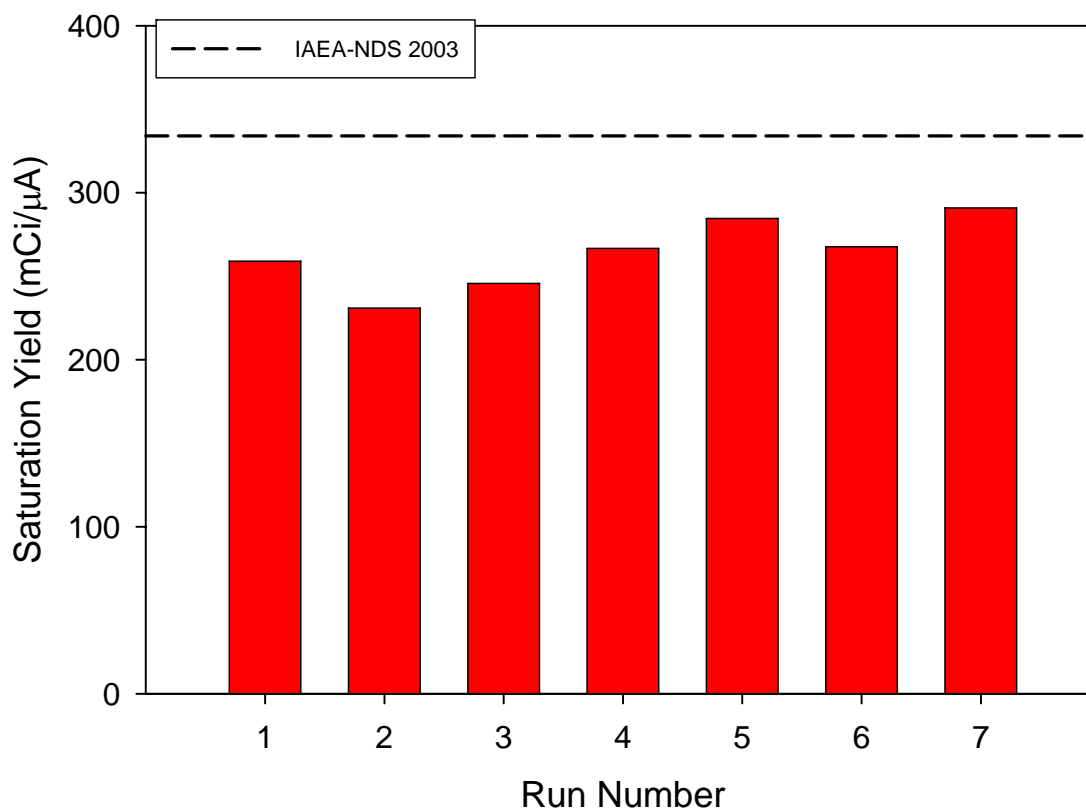
Figure 6-9: Summary of ^{18}F Yield Data

Table 6-2: Summary of ^{18}F Yield Data

Run	Date	Nuclear Reaction	I_{beam} (μA)	IT (min.)	Sat. Yield (mCi/μA)
1	12/5/2007	$^{18}O(p,n)^{18}F$	5	30	259.0
2	12/6/2007	$^{18}O(p,n)^{18}F$	25	87	230.9
3	12/6/2007	$^{18}O(p,n)^{18}F$	30	45	245.7
4	12/9/2007	$^{18}O(p,n)^{18}F$	30	60	266.7
5	1/3/2008	$^{18}O(p,n)^{18}F$	35	60	284.6
6	1/3/2008	$^{18}O(p,n)^{18}F$	35	30	267.7
7	1/10/2008	$^{18}O(p,n)^{18}F$	30	30	290.9
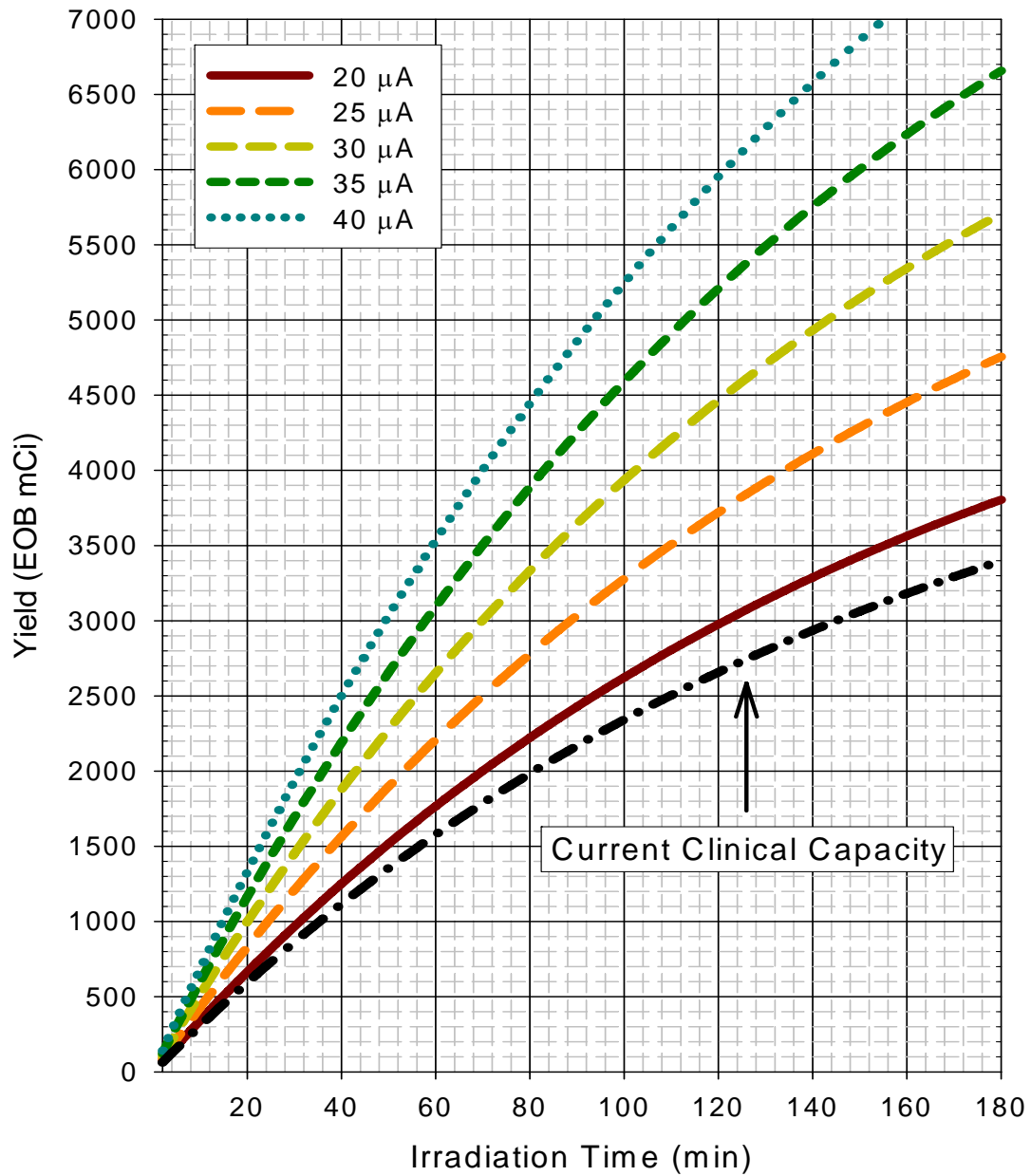
Figure 6-10: Production Capabilities of TS6-DUKE System

6.2 TS6-WMC

TS6-WMC was the first thermosyphon system designed specifically for the PETtrace cyclotron. The key design features are based on the TS6 Duke target but with a 15 mm diameter chamber 15 mm deep. The chamber volume is 4.2 cc, resulting in an average consumption of 5.0 cc per irradiation. The target insert was constructed of silver due to ease of fabrication and lead time concerns.

6.2.1 D-PACE Short Port Collimator and Alignment Diagnostics

The target was installed in tandem with a short port 4-jaw collimator designed and fabricated by Dehnel Particle Accelerator Components Engineering (D-PACE). This device contains four overlapping water-cooled graphite segments which can be sized to form a 12, 13, 14 or 15 mm aperture. Beam current is measured on each segment independently. This provides information about beam transmission as well as shape and spill in two dimensions. The device is shown installed on the horizontal target port in Figure 6-11, and as an isometric drawing in Figure 6-12.
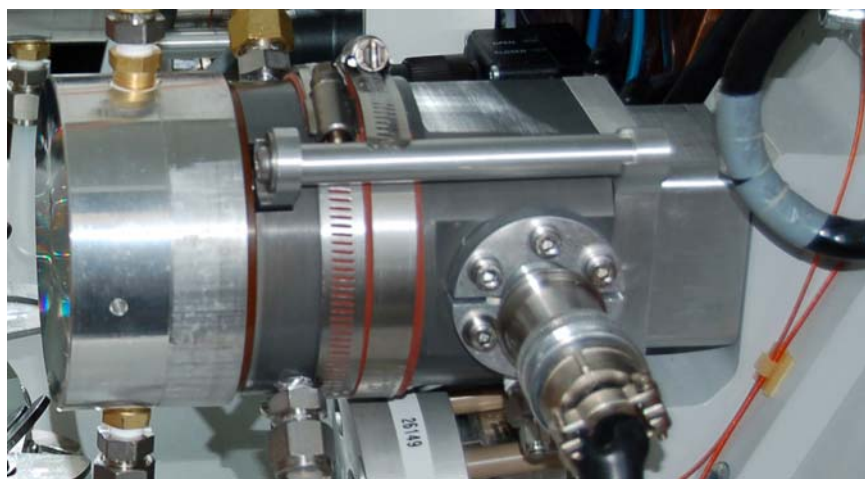
Figure 6-11: Short Port Collimator Installed on GE PETtrace
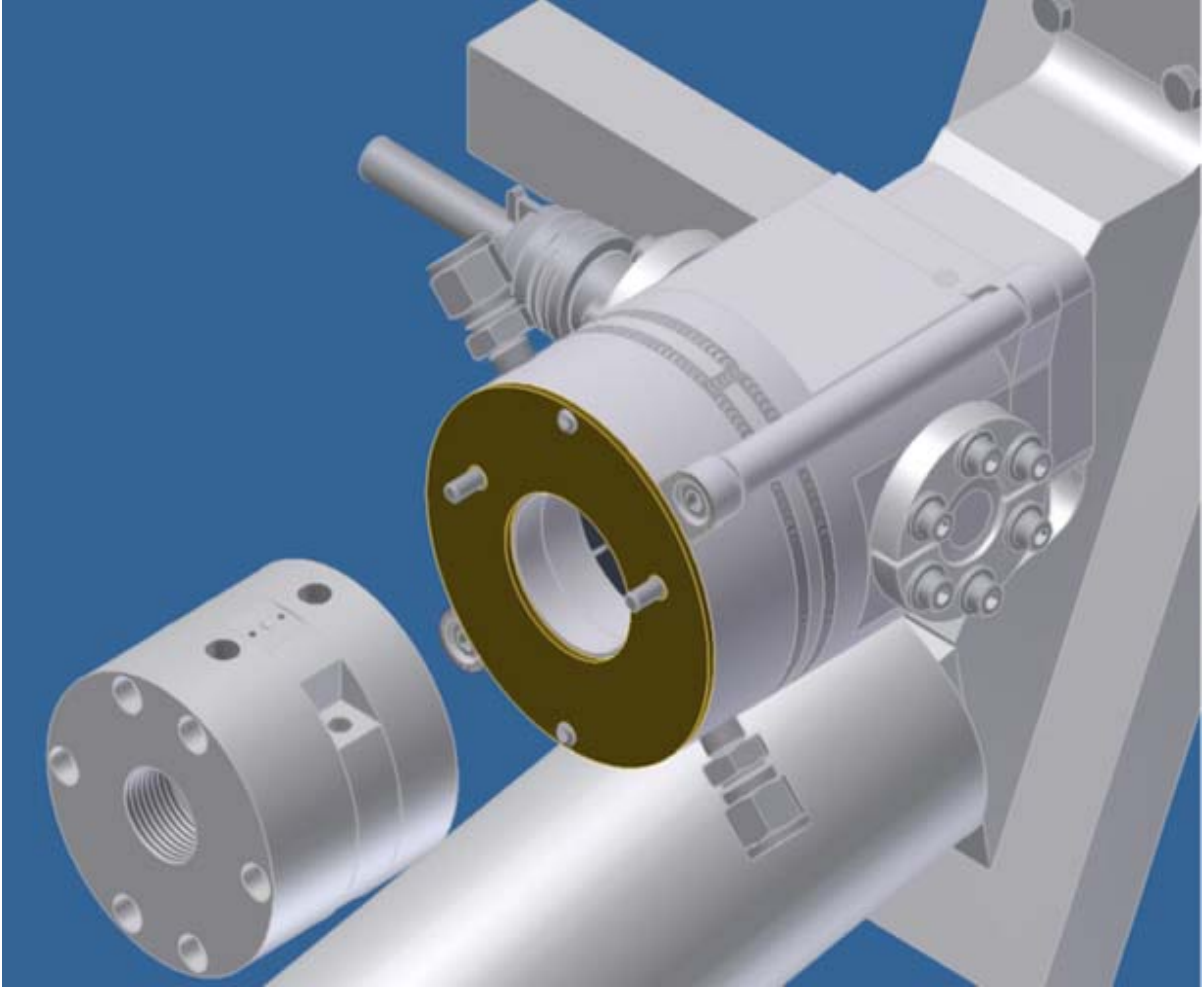
Figure 6-12: Short Port Collimator and Target (D-PACE 2006)

Before installing the external collimator assembly, the internal beam port hardware needed to be configured. The PETtrace beam channel analyzer (BCA) measures beam currents from the target as well as a two segment collimator inside the vacuum tank wall. These signals are used for feedback in the stripper foil positioning algorithm while running automated production. The internal collimator segments were installed in a starting position specified by the GE documentation. Paper burns were then performed as a basis for alignment adjustments (Figure 6-13).

49
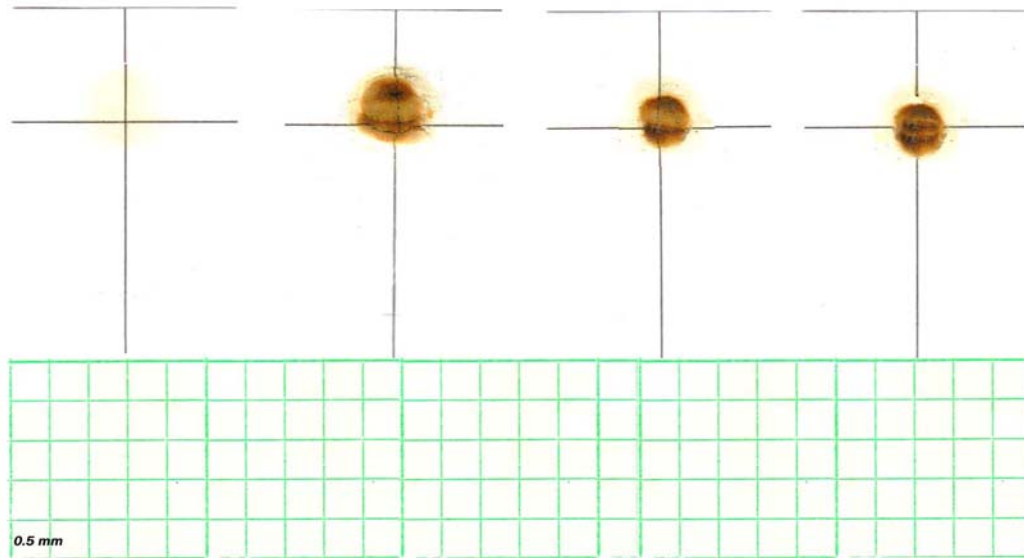
Figure 6-13: Beam Alignment with Paper Burns

The short port was assembled and installed with the 12 mm aperture. A high current Faraday cup was placed in the target position and connected to the BCA. The BCA does not include any additional channels, so external collimator currents were amplified to a level appropriate for the FieldPoint analog inputs with an intermediate conditioning circuit. A low-pass RC network was also placed close to the target in each current channel to filter noise.

Beam was acquired on the diagnostic target, and a series of low power vertical sweeps were performed to ensure that the alignment of the components was optimum. This is accomplished by indexing the stripper foil position. The process begins with the beam incident completely upon the lower (or upper) internal collimator segment. As the stripper foil position is indexed, the beam projection moves up (or down) in discrete increments. As the beam edge extends beyond the internal collimator, it is incident upon the first vertical segment of the external collimator. As the process continues, the beam moves onto the target

50

and all four collimator segments. The goal of this exercise is to achieve an equal ratio of internal and external currents on the vertical segments and balanced currents on the two horizontal segments at the point of maximum transmission. This concept can be described more easily graphically. Figure 6-14 shows the current signals from the target and collimators as a function of beam current for the aligned assembly.
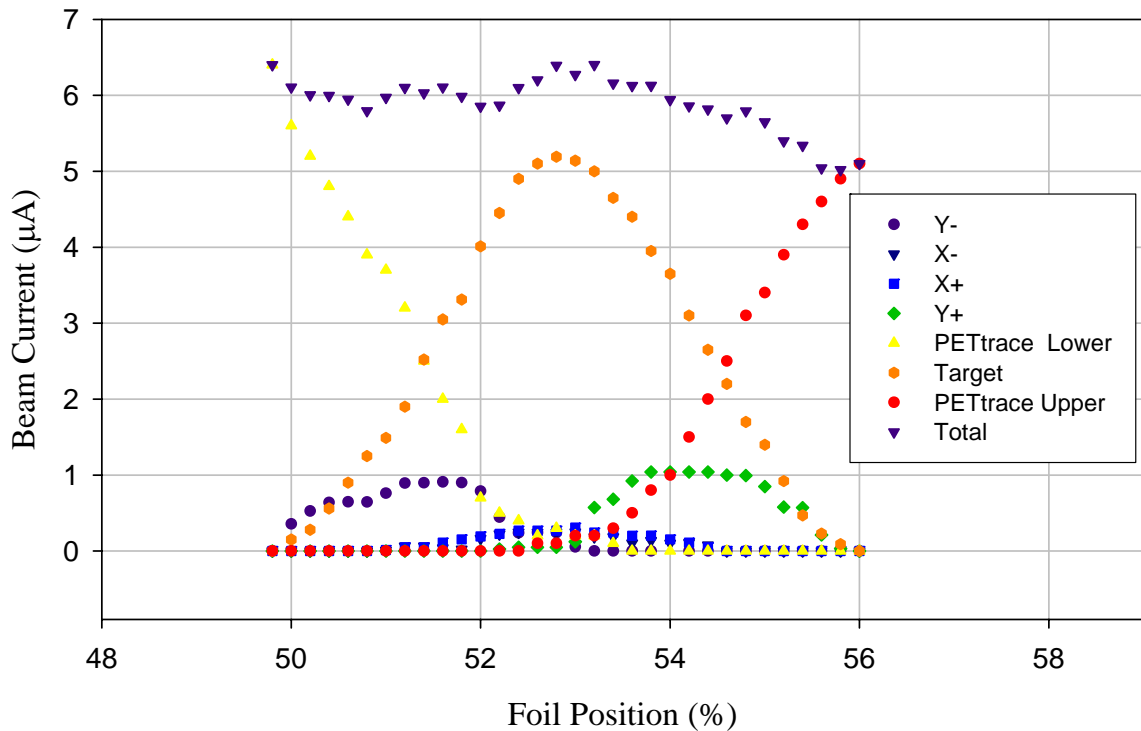
Figure 6-14: Beam Sweep Exercise

Transmission data were recorded for beam intensities up to 110 µA on target. Unfortunately, due to limitations of the BCA circuitry, the stripper foil current can only be measured for values up to 100 µA. Because of this limitation, the true transmission is unknown for this experiment at intensities above approximately 80 µA on target. Consequently, the maximum target current for automated production is also limited to 80 µA.

It is certain that transmission could be improved by installing a larger collimator aperture, but this was not pursued due to time constraints. The transmission data are included in Figure 6-15.
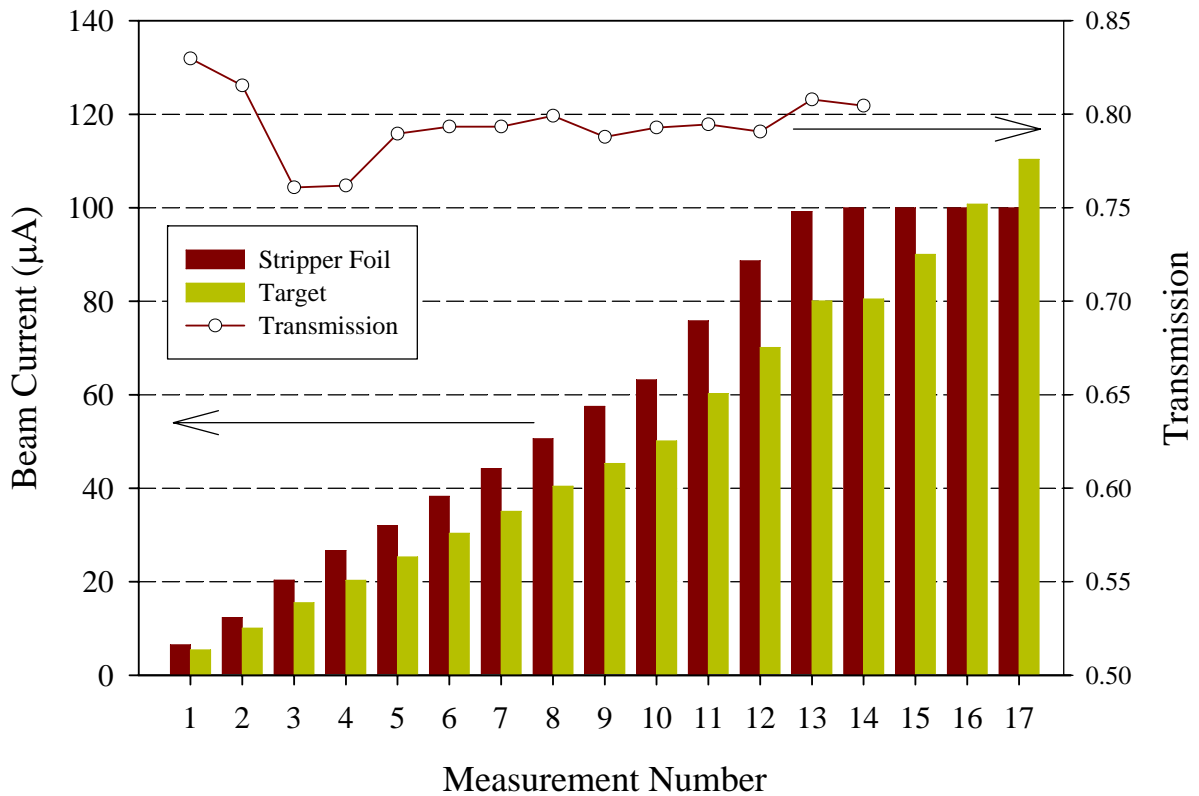
Figure 6-15: Transmission of Collimator Assembly

In the case of early PET cyclotrons, such as the RDS-112 or CS-30, the beam shape is tunable by many mechanisms including fine adjustment of the ion source position. It was assumed that online ion source adjustments could be made on the PETtrace as well, and that the external collimator could be used to achieve a favorable distribution of particles on target. This was not the case, however, as ion source adjustment on the PETtrace is a procedure that

52

requires opening the vacuum tank. Consequently, the collimator was of less utility than had been anticipated.

The final diagnostic exercise conducted before installing the thermosyphon involved acquiring beam on a quartz disc. As the high energy protons slow down in the disc, the Cerenkov Effect produces visible light. Since the disc is transparent, this can be observed by placing a video camera inside the cyclotron shield doors. The images of this projection on the disc give information about the extent of the beam, as well as some qualitative information about the distribution. This information is useful, but since the disc is very susceptible to thermal stress, these experiments are limited to beam intensities less than 1 µA. Quantitative analysis of the distribution has been reserved for later work. An example of an illuminated target is shown in Figure 6-16. The image is shown as a negative for clarity. The bright outer ring is due to illumination of the housing material.
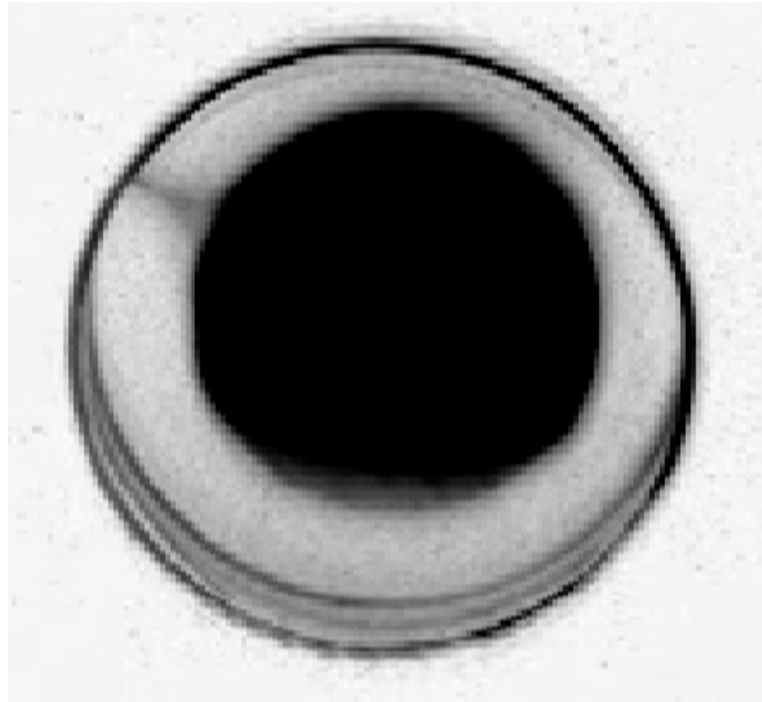
Figure 6-16: Image of the PETtrace Beam Projection on a Quartz Disc

53

These experiments gave an approximate beam spot size at a target equivalent distance from the stripper foil. Since the outer ring has a diameter of 17 mm, the beam diameter was estimated to be 13 mm or less. Unfortunately, experiments performed on later targets have since shown that chamber diameters less than 15 mm are susceptible to geometry losses due to increased beam divergence at high intensity.

6.2.2 Cooling Flow Characterization

Due to space limitations, it was not possible to install inlet and out manifold connections for measuring the cooling flow pressure drop across the target. Therefore, cooling flow rates could not be measured during irradiation. Instead, the flow in each cooling circuit was measured with the shield doors open using a mechanical flow meter. The flow rates are included in Table 6-3.

Table 6-3: Cooling Flow Rates for TS6-WMC

Flow Circuit		Flowrate	
		GPM	lb_m/sec
Radial Channels		1.83	0.25
Rear Jet		2.43	0.34

6.2.3 Sight Tube Analysis

Sight tube data were collected at a beam energy of 16.5 MeV and an overpressure of 400 psig. These experiments were performed from the PETtrace service computer which permits higher power operation but removes many protective interlocks. The limiting component for this mode of operation is the radiofrequency power supply, which cannot exceed 15 kW. This corresponds to roughly 150 µA of beam at the exit port. After

54

transmission losses through the collimators, it was possible to obtain a maximum of 125 μA on target.

The target exhibits typical behavior in the thermal expansion, subcooled boiling and bulk boiling modes up to 110 μA (1760 W). Above this power level, the incremental rise in sight tube level becomes smaller with respect to constant increases in current (Figure 6-17). It was initially hypothesized that this behavior results from an increase in condenser void fraction and the subsequent increase in condensing heat transfer coefficient. Later targets have since shown this behavior very close to the onset of target penetration. While the target insert exhibited some discoloration, it was not clear that significant penetration had occurred (Figure 6-18). In order to conclusively determine the cause, it will be necessary to perform yield tests at these elevated currents.
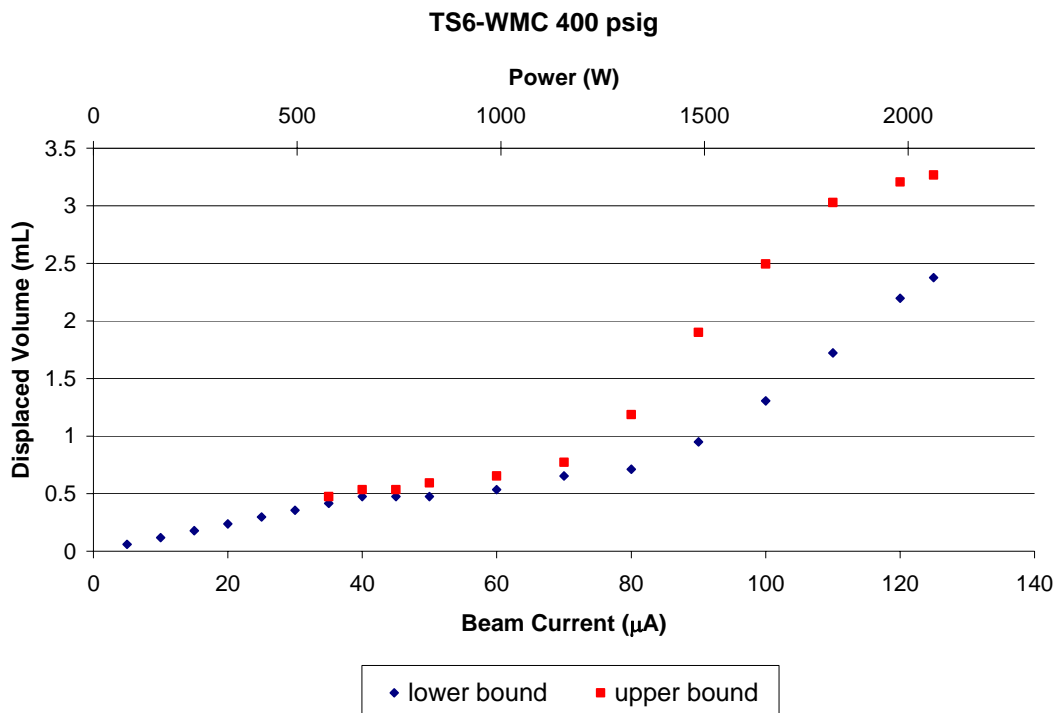
Figure 6-17: TS6-WMC Sight Tube Data

55
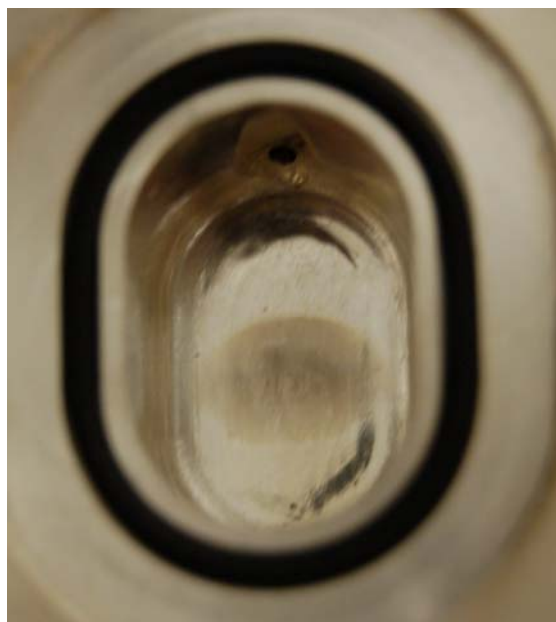
Figure 6-18: TS6-WMC Target Insert Post-Irradiation

6.2.4 Radiochemical Yield

Yield experiments were performed at beam intensities up to 80 μA. Unfortunately, the automated production mode currently only supports beam currents up to 100 μA (80 μA after transmission in this instance). It is possible, though tedious, to perform lengthy irradiations from the service computer. Future work will include yield measurements at higher beam currents.

A natural abundance water irradiation was first performed at 80 μA to acquire an additional transmission benchmark. In this case, the water was degassed ultrasonically to mitigate volatile ^{13}N production as an alternative to using a dilute ethanol mixture. The PETtrace beam energy (16.5 MeV) is conveniently shy of the threshold energy (16.6 MeV) for the ^{16}O(p,pn)^{15}O nuclear reaction. This simplifies analysis of the ^{13}N decay data considerably as the source produced is effectively monoisotopic.

56

[O-18]enriched water irradiations were performed at 80 µA. The automated production algorithm provided reasonable balance of collimator currents for the length of both irradiations. The third batch was used to synthesize FDG with a GE TracerLab MX unit. The decay corrected post-synthesis FDG yield was well within normal specifications at a value of 69%. Results from yield test irradiations are included in Table 6-4.

Table 6-4: TS6-WMC Yield Summary

Run	Date	Nuclear Reaction	I_{beam} (µA)	IT (min.)	Sat. Yield (mCi/µA)
1	6/14/2007	$^{16}O(p,\alpha)^{13}N$	80	20	37.3
2	6/15/2007	$^{18}O(p,n)^{18}F$	80	30	249.8
3	6/15/2007	$^{18}O(p,n)^{18}F$	80	60	241.7

Production estimates for the TS6-WMC target system are included in Figure 6-19. This system offers significant production gains when compared to the standard GE targets. A standard target irradiation at WMC is 35 µA for 120 minutes, with a saturation yield of 230 mCi/µA. The GE targets can also be run in parallel with dual beam extraction for an effective beam current of 70 µA. For a conservative irradiation at 75 uA, the fluoride yield from the TS6-WMC is an improvement of more than 25% over a standard dual target irradiation. At 100 µA, the gain would be approximately 70%.

This target system is not optimal for routine production due to its relatively large footprint and interference with the preexisting target in position one. The fundamental design, however, is certainly adaptable to a more fully engineered solution for the PETtrace application. This was the goal during the next phase of the project.

57
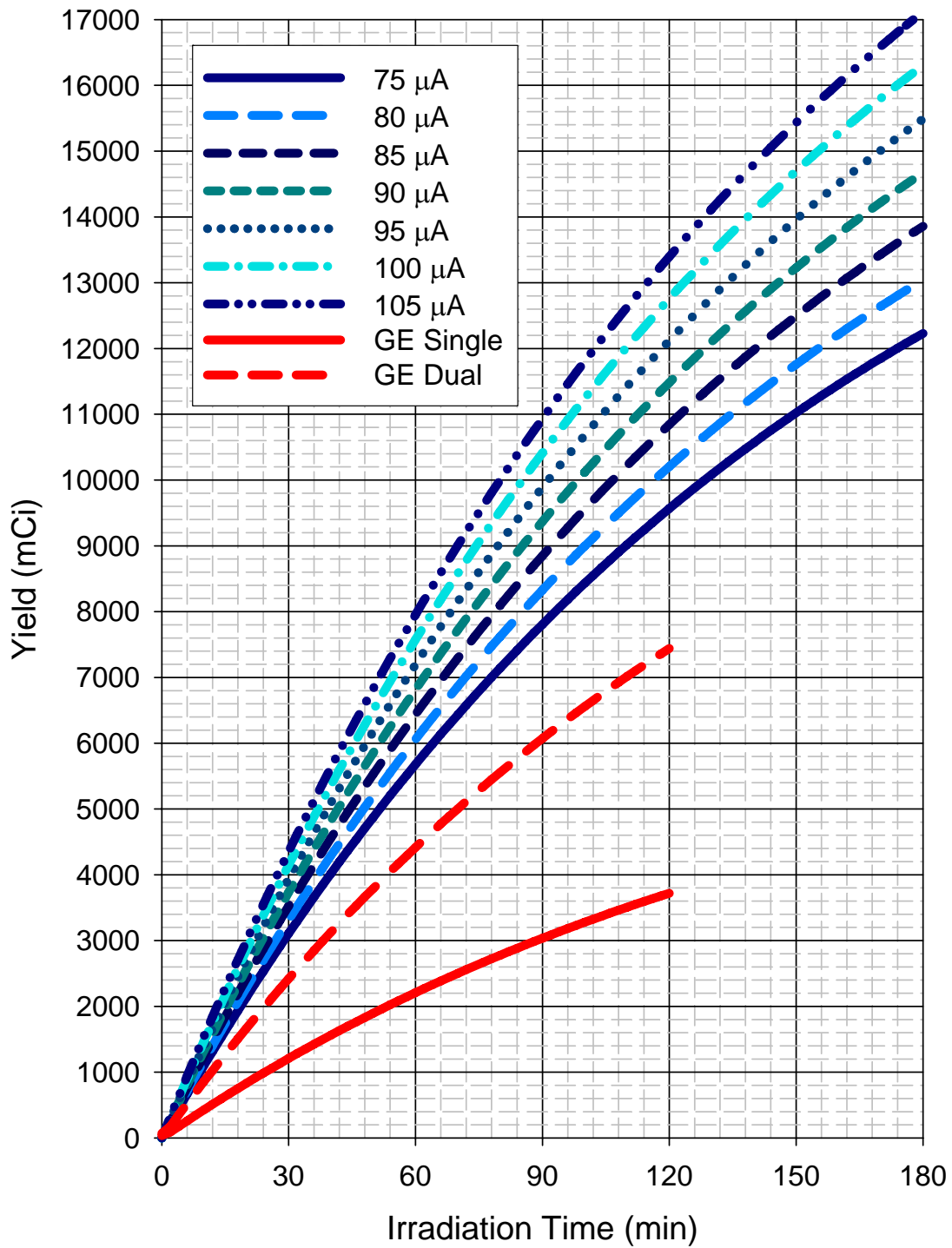
Figure 6-19: Production Capabilities of TS6-WMC System

6.3 TS7-WMC

The TS7 target was designed by Bruce Technologies, Inc. as a prototype retrofit system for the PETtrace. The objectives were further integration into the PETtrace systems and reduced chamber volume. The connections to the beam port and chilled water header are identical to those found in GE targets (Figure 6-20 and Figure 6-21).
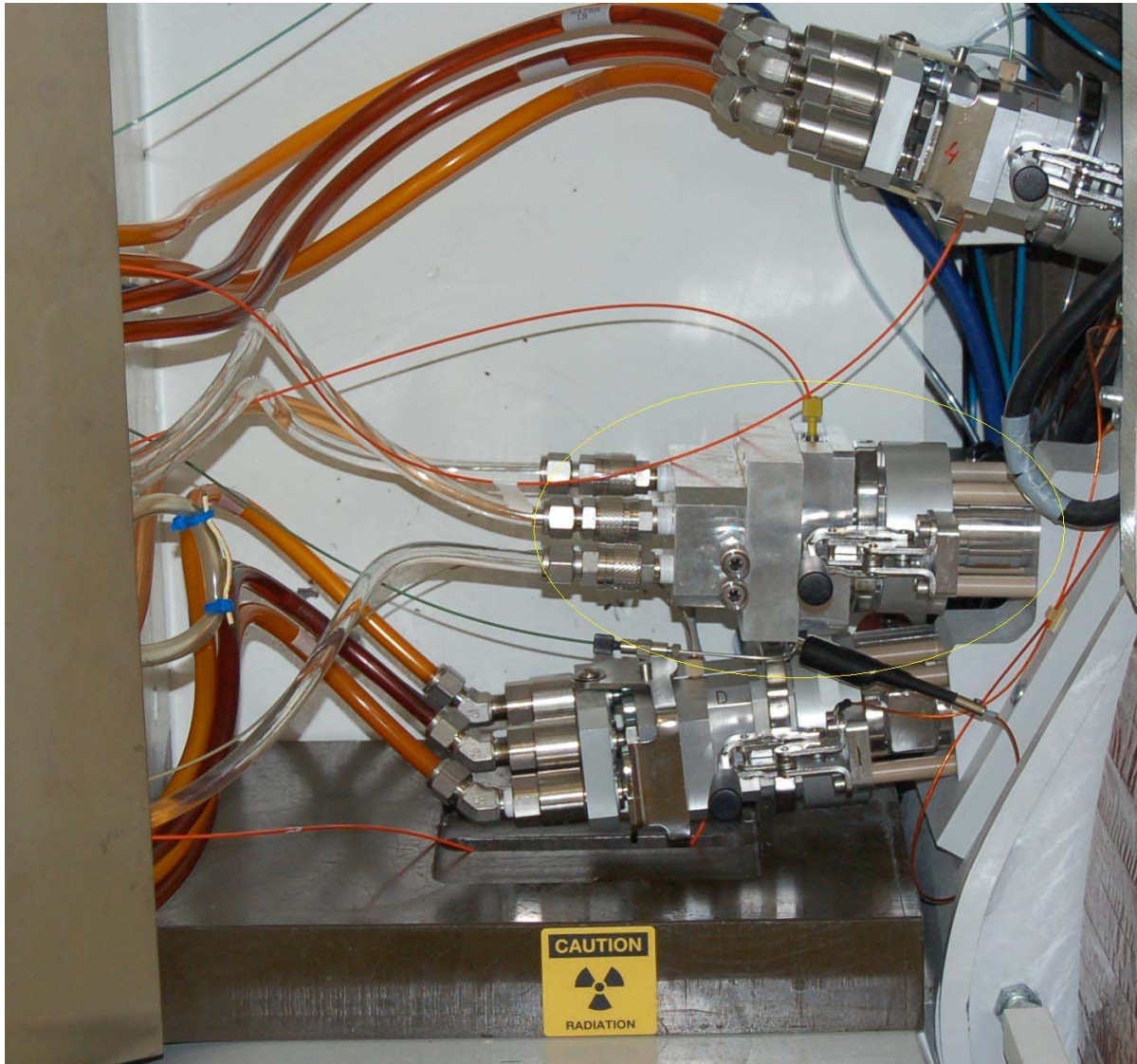
Figure 6-20:TS7-WMC Installed on PETtrace Beam Port (Position 2)

The chamber volume was reduced to 3.2 cc with an enriched water consumption of 4.0 cc per irradiation. The decision to reduce the chamber dimension was motivated by the reservoir capacity of the TracerLab MX synthesis system. This was ill-advised, since the amount of resulting performance reduction was not clear. It has since been concluded that the synthesis system should instead be tailored to suit a larger volume.

This platform utilized a target insert similar to the TS6 targets. The first target insert was constructed of silver. Tantalum inserts were fabricated two months later.
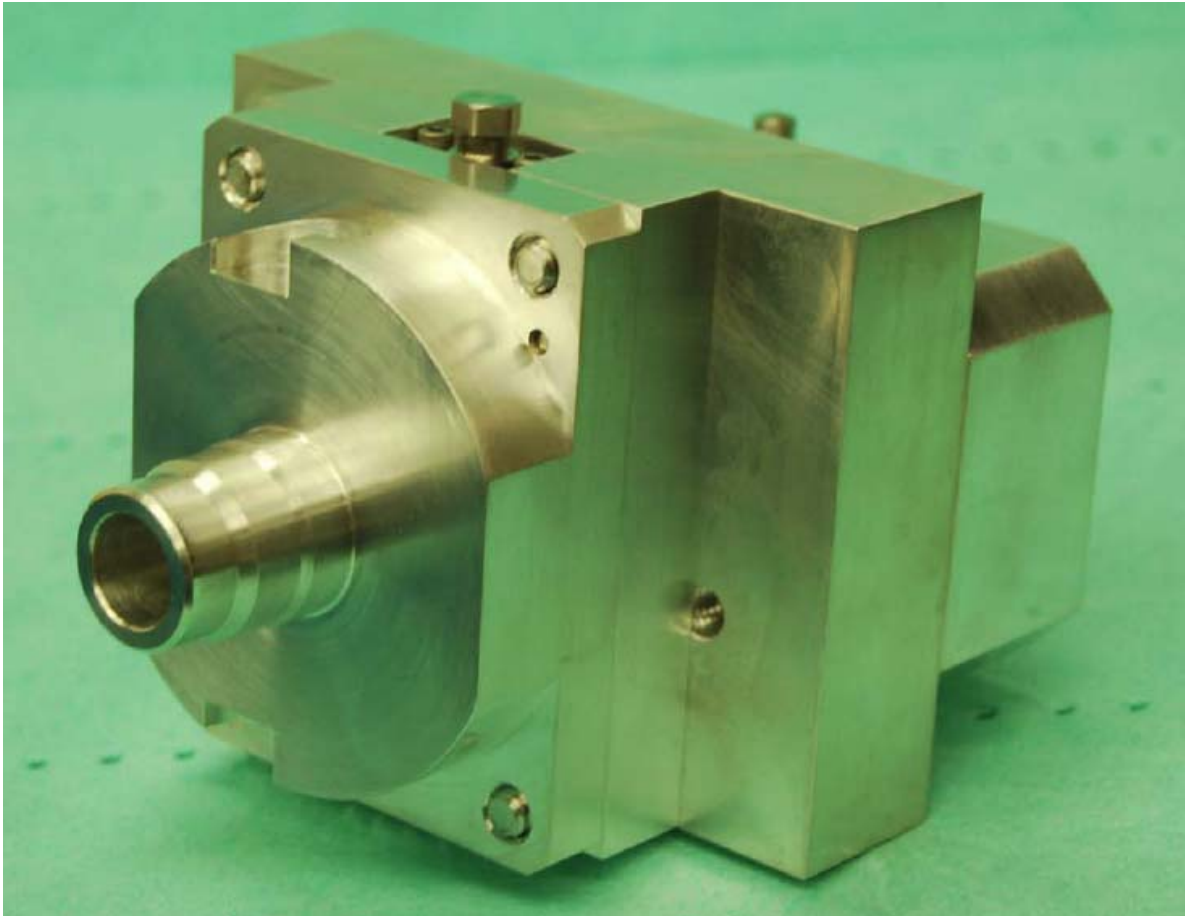
Figure 6-21: TS7-WMC Assembled Target

The geometry of the radial cooling channels is very similar to TS6 designs (Figure 6-22). These channels are spaced uniformly, 0.045" from the chamber wall. The channel diameter is 0.055". The axial cooling arrangement, however, was redesigned to accommodate a serial flow path. This is discussed in more detail in the following section.
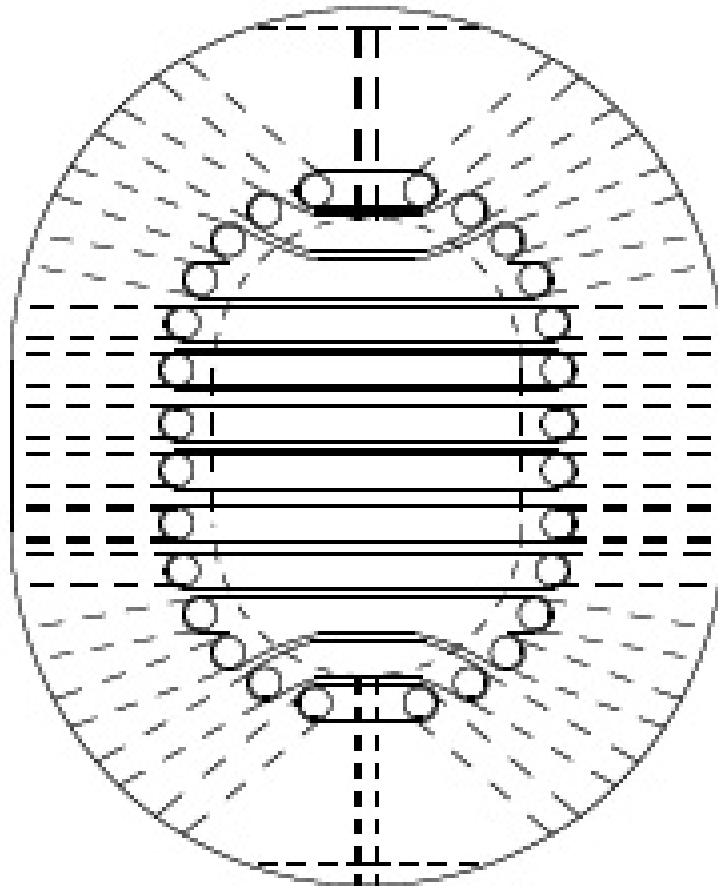
Figure 6-22: TS7 Target Insert

61

6.3.1 Cooling Flow Characterization

The cooling manifold design of the TS7 target was limited by the standard PETtrace service connections. However, since helium window cooling is not used, all four ports on the connecting block could be used for cooling water. Space considerations dictated a serial cooling arrangement. The radial cooling channels were connected with horizontal slots on back of the target insert. This provided structural support so that the back wall could be machined thinner, reducing conduction distance. The cooling water is directed into the slots using a rectangular vertical manifold. The drawback to this arrangement is significant variation in the radial channel velocities.

In order to better understand this behavior, fluid simulations were performed using the ANSYS CFX software package [1]. The slotted arrangement was compared with a smooth back and jet, similar to TS6. The relative velocity for each radial channel was calculated for each of the two cases. Results from this exercise are included in Figure 6-23 and 6-24.
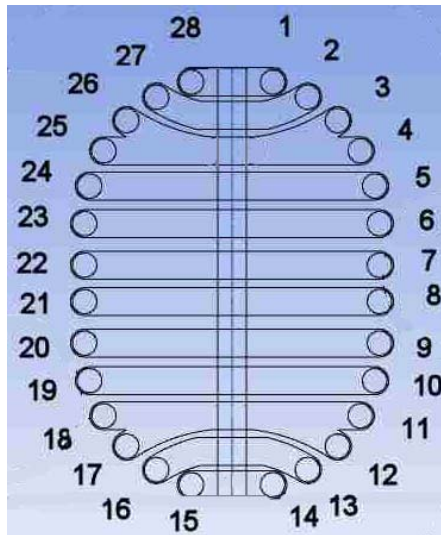
Figure 6-23: Channel Numbering Scheme (Mark Humphrey 2007)

62

The overall target forms loss was also measured directly. Rather than measure differential pressure across the target in an external manifold, pressure equalization channels were drilled in the rear target flange. The penetrations created by this modification were fitted with dry break quick disconnects and connected to the differential pressure transducer via static lines. A drawing of the rear flange is included in Figure 6-25. These connections can also be seen in Figure 6-20.
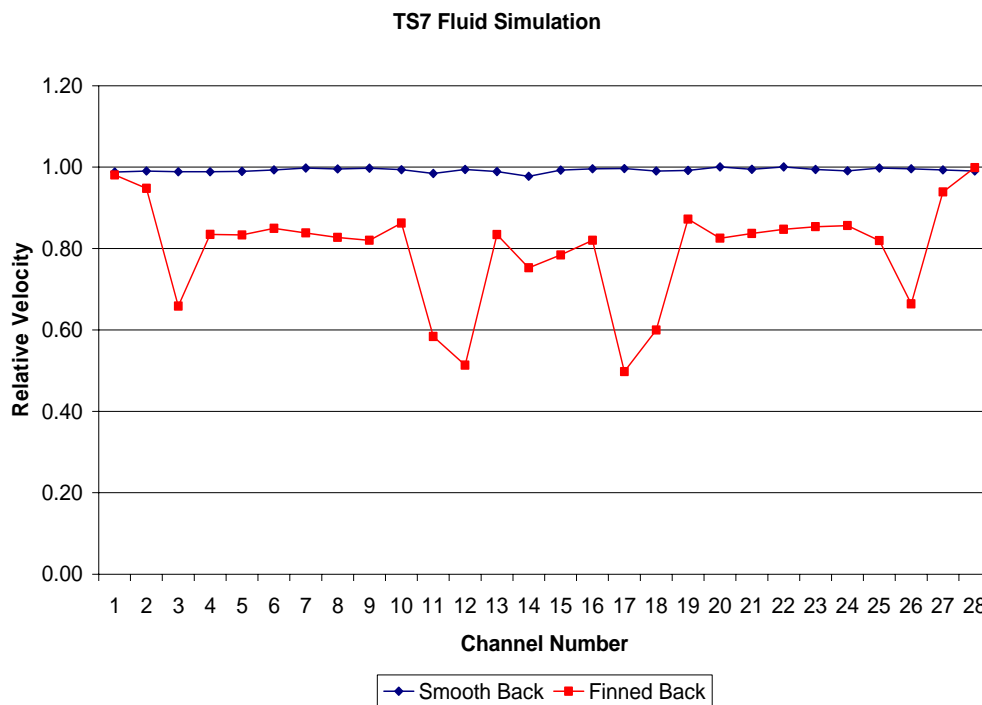
Figure 6-24: TS7-WMC Fluidic Simulation (Mark Humphrey 2007)

As with previous targets, the cooling flow as a function of differential pressure for the target was measured experimentally at North Carolina State University. After installing the target on the PETtrace cooling header, differential pressure measurements were taken under single supply and return as well as dual supply and return conditions. The data from this exercise is included in Figure 6-26.

63
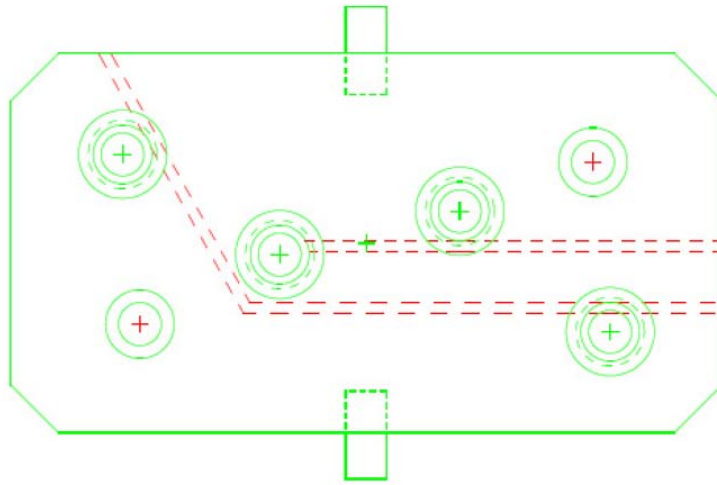
Figure 6-25: TS7 Rear Cooling Water Manifold

Flow vs. Pressure Drop TS7
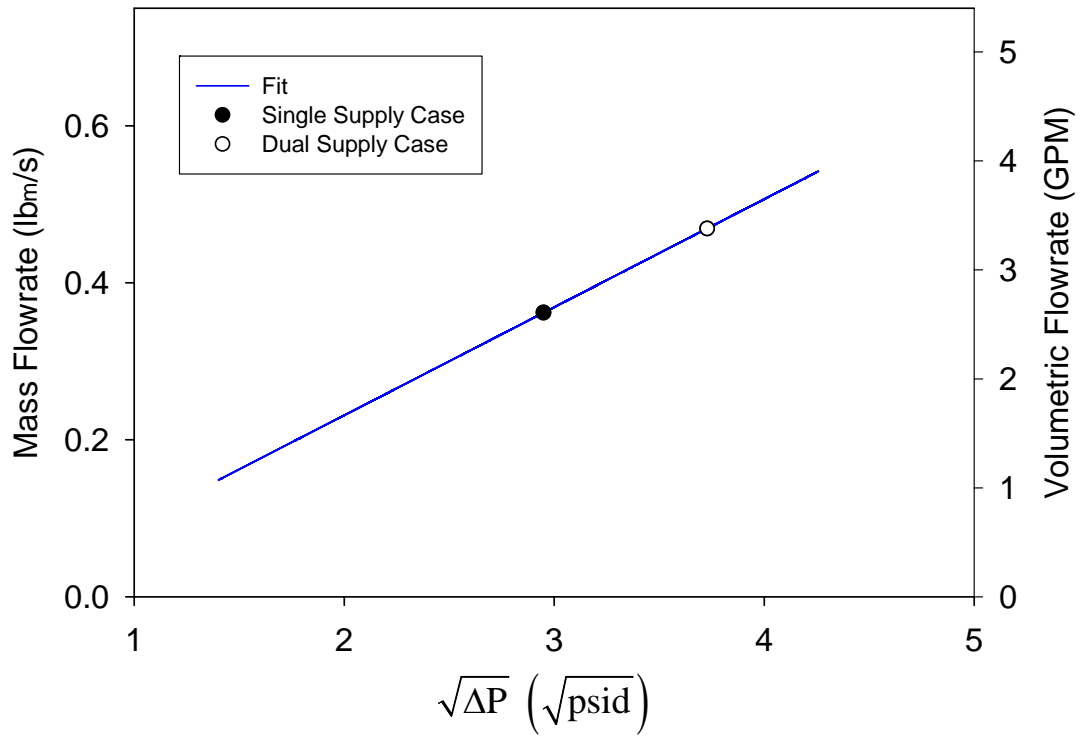
Figure 6-26: Cooling Water Flow as a Function of Target Pressure Drop

64

6.3.2 Sight Tube Analysis

Sight tube irradiations were performed on natural abundance water for both silver and tantalum target inserts. The TS7-WMC mounts directly on the exit port of the vacuum tank resulting in fewer transmission losses to target than the previous system. Consequently, it was possible to obtain beam intensities as high as 140 µA on target. Data from these experiments are included in Figure 6-27 and Figure 6-28.

The displaced volume of liquid from the silver insert was proportionately lower than the tantalum insert for the range of intensities investigated. This was expected due to the much higher thermal conductivity of silver. Ultimately, any additional resistance to heat transfer is reflected by an increased vapor fraction in the target medium. In both instances,
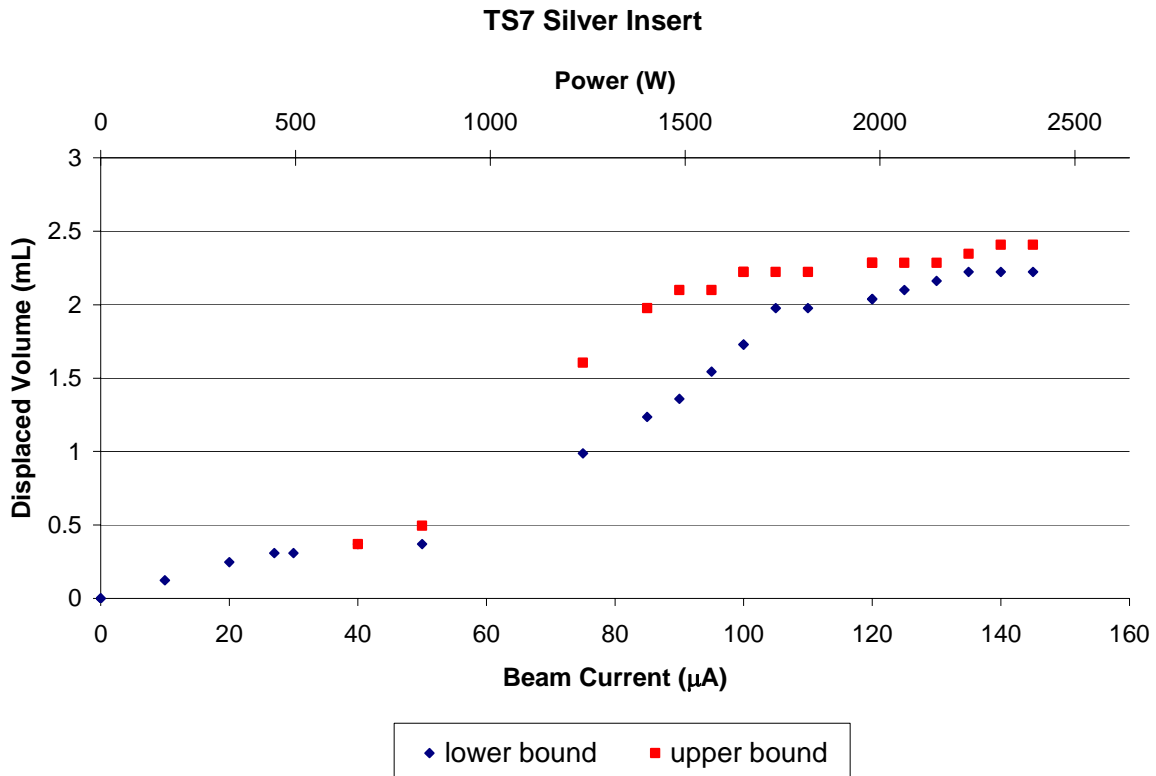
Figure 6-27: TS7-WMC Silver Insert Sight Tube Data

65

TS7 Tantalum Insert
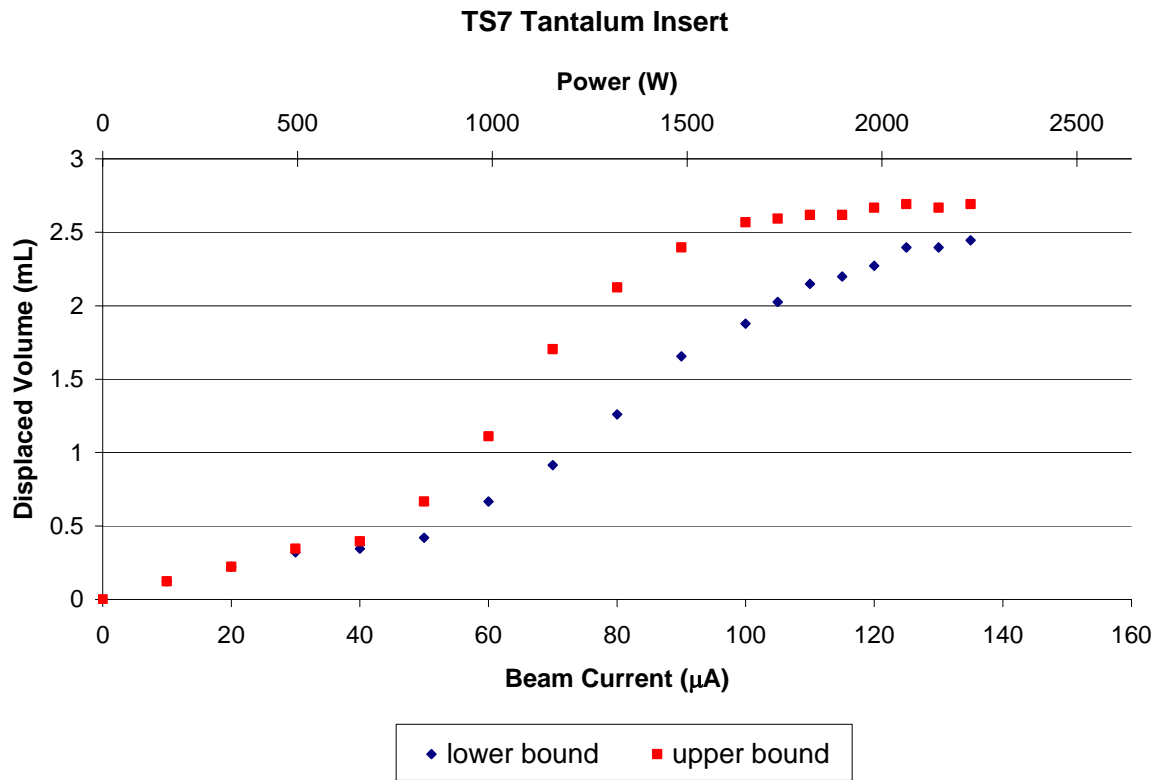
Figure 6-28: TS7-WMC Tantalum Insert Sight Tube Data

the slope of the curve representing displaced volume with respect to beam intensity gradually decreases at elevated current. This occurs at lower power for the tantalum insert, which supports the possibility of target penetration.

Visual inspection of both inserts shows evidence of significant heating in the target back (Figure 6-29). Additionally, the target inserts and front target flange showed evidence of heating on the left and right sides. This suggests the possibility of reduced transmission due to the 13.5 mm chamber diameter.

66

Figure 6-29: TS7 Silver Insert Post-Irradiation

6.3.2 Radiochemical Yield

6.3.2.1 Silver Insert Yield Results

The first two natural abundance yield tests produced near theoretical results at 100 µA. During the third test, the target was irradiated without cooling water for a brief period and subjected to very high temperature. This was, of course, unintentional and occurred while operating from the service computer, where many protective interlocks are disabled. While the target remained mechanically intact, the silver surface was heavily oxidized during the event. A complete cleaning of the system including the target, associated valves and plumbing was performed to mitigate contamination. All of the target o-rings and PEEK tubing were also replaced.

67

Subsequent natural abundance yield tests were performed at beam currents up to 100 μA. These yields were marginally lower than had been seen with the TS6-WMC target. It is presently unclear whether this is a function of transmission losses or contamination in the target filler. Typically ^{13}N is less susceptible to poor chemistry than ^{18}F but it appears that contamination can lead to increased ^{13}N$_2$ production. Natural abundance yield results are included in Table 6-5.

Table 6-5: TS7-WMC Silver Insert ^{13}N Yield Summary

Run	Date	Nuclear Reaction	I_{beam} (μA)	IT (min.)	Sat. Yield (mCi/μA)
1	9/2/2007	$^{16}O(p,\alpha)^{13}N$	100	30	35.7
2	9/2/2007	$^{16}O(p,\alpha)^{13}N$	100	30	31.4
3	9/3/2007	$^{16}O(p,\alpha)^{13}N$			LOCA
4	9/3/2007	$^{16}O(p,\alpha)^{13}N$	100	30	13.4
5	9/4/2007	$^{16}O(p,\alpha)^{13}N$	100	30	31.5

Saturation yields performed with [O-18] enriched water were also lower than observed with TS6-WMC. The performance appears to be a function of beam intensity, as the lower intensity irradiations produced higher saturation yields. Due to the physical appearance of the silver insert, the simplest explanation is the onset of target penetration at intensities approaching 100 μA. However, if penetration were the only complicating factor, irradiations at low intensity should produce near theoretical saturation yield (250 mCi/μA). This is not the case (Table 6-6), which suggests that either poor transmission or contamination is also present.

68

Table 6-6: TS7-WMC Silver Insert ^{18}F Yield Summary

Run	Date	Nuclear Reaction	I_{beam} (μA)	IT (min.)	Sat. Yield (mCi/μA)
1	9/5/2007	$^{18}O(p,n)^{18}F$	100	60	197.5
2	9/5/2007	$^{18}O(p,n)^{18}F$	100	60	193.9
3	9/5/2007	$^{18}O(p,n)^{18}F$	50	60	212.5
4	9/6/2007	$^{18}O(p,n)^{18}F$	100	60	185.0
5	9/7/2007	$^{18}O(p,n)^{18}F$	100	60	191.6
6	9/8/2007	$^{18}O(p,n)^{18}F$	85	60	203.8

6.3.2.2 Tantalum Insert Yield Results

While prototyping the inserts with silver yields useful data, the ultimate goal has always been to take advantage of the chemical properties of tantalum. In this instance the insert material is especially critical, because silver chemistry poses a potential degradation in performance and introduces additional unknowns.

Though it was not an issue during initial sight tube characterization, two window failures occurred during the initial natural abundance water irradiations. It was initially hypothesized that a poor chamfer finish on the clamping ring was the case. The chamfer radius was increased and polished on a cold target assembly. Window burst tests were performed using the test target and the cold target. In both instances, the foils ruptured at approximately 800 psig.

Upon further investigation of the target insert and failed foils, it became apparent that the failure was initiated preferentially in the left side of the target. Due to the small radius of the insert, there is a small portion of beam incident on the chamber sides and entry port. This

69

could potentially lead to localized heating of the clamping surfaces and weakening of the window material. A thicker window (0.002") was installed to add pressure margin. This was controversial, because increasing the window thickness increases the energy deposition in the window and could potentially accelerate failure due to critical heat flux. Fortunately, the thicker window has maintained its integrity for more than 3500 µA-hours since installation.

Natural abundance water irradiations produced saturation yields comparable to data collected from the silver target insert. The irradiations were performed at beam intensities up to 90 µA. Due to the facility production schedule, it was decided not to exceed this power level and risk machine downtime from additional window failures. A low intensity irradiation at 50 µA was used to achieve an initial benchmark. Current was increased gradually over the course of the following eight irradiations. Data from these experiments are included in Figure 6-30 and Table 6-7.

It is unclear what caused the drastic reduction in yield at 90 µA. A significant component of gaseous activity was noted immediately after delivery. A fraction of this activity was not exhausted and diffused into the lab. Area monitors soon exceeded dose rate alarm levels, and it was necessary to seal the hot lab while the activity decayed. All other irradiations appeared consistent.

70

TS7 ^{13}N Saturation Yields Tantalum Insert
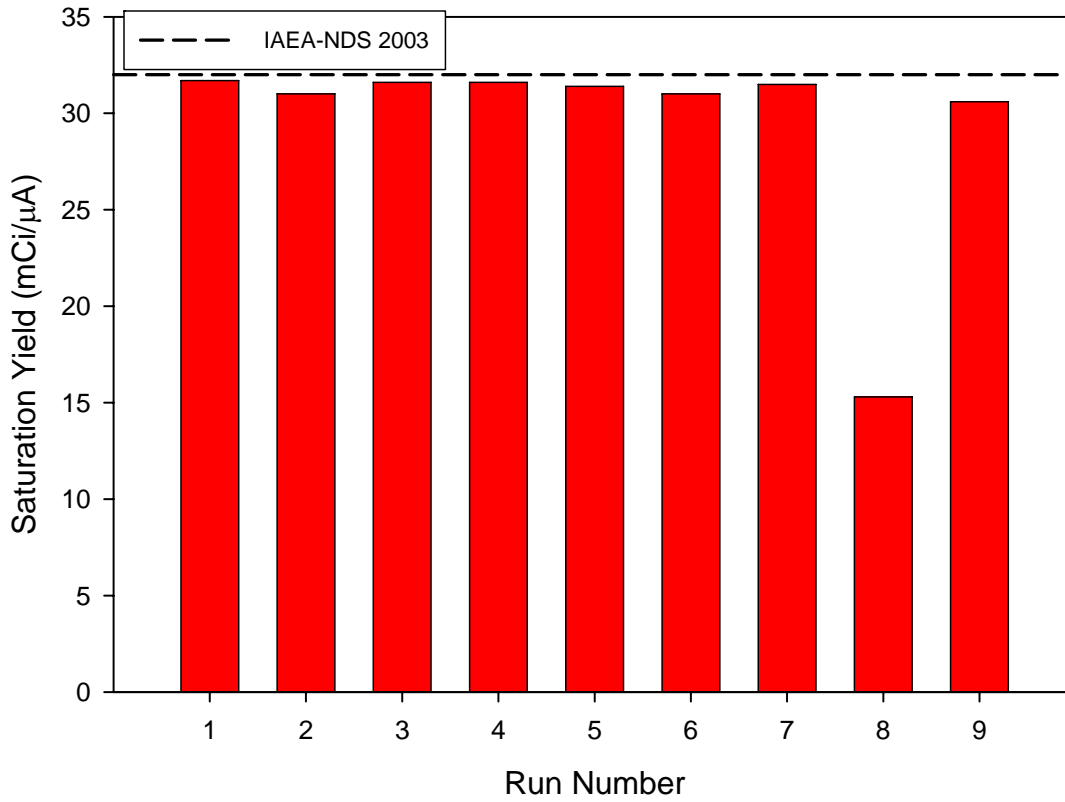
Figure 6-30: TS7-WMC Tantalum Insert ^{13}N Yield Summary

Table 6-7: TS7-WMC Tantalum Insert ^{13}N Yield Summary

Run	Date	Nuclear Reaction	I_{beam} (μA)	IT (min.)	Sat. Yield (mCi/μA)
1	1/11/2008	$^{16}O(p,\alpha)^{13}N$	50	20	31.7
2	1/11/2008	$^{16}O(p,\alpha)^{13}N$	70	20	31.0
3	1/11/2008	$^{16}O(p,\alpha)^{13}N$	75	20	31.6
4	1/11/2008	$^{16}O(p,\alpha)^{13}N$	80	20	31.6
5	1/11/2008	$^{16}O(p,\alpha)^{13}N$	85	20	31.4
6	1/11/2008	$^{16}O(p,\alpha)^{13}N$	85	20	31.0
7	1/12/2008	$^{16}O(p,\alpha)^{13}N$	85	20	31.5
8	1/12/2008	$^{16}O(p,\alpha)^{13}N$	90	20	15.3
9	1/12/2008	$^{16}O(p,\alpha)^{13}N$	85	20	30.6

71

Irradiations were performed with [O-18]enriched water at intensities up to 85 μA. Saturation yields were comparable to data obtained with the silver target insert. If penetration onset were present at 90 μA, we would expect more of a yield reduction at 85 μA. Data are included in Figure 6-31 and Table 6-8. Again, further irradiations at higher power will be necessary to conclusively determine penetration.

Batches six, seven and nine were synthesized into FDG, analyzed using standard facility QC procedures, and used for target system qualification. These batches were delivered directly into a TracerLab MX unit, and were not assayed in the dose calibrator. If decay corrected post-synthesis yields of 70% are assumed, the saturation yields from these irradiations are consistent.

One item of particular interest from these experiments is the lack of reduction in yield from extended irradiation time. Typical irradiation lengths for silver targets are limited to 120 minutes or less. Running longer causes accelerated chamber wear, which can significantly shorten the lifespan of a target insert. In the case of the three hour and four hour batches, the saturation yields were consistent with shorter runs at similar intensities. The net yield from run 12 exceeded 11 Ci at EOB, with over 10.5 Ci recovered in the dose calibrator 10 minutes later (Figure 6-32).

TS7 Saturation ^{18}F Yield Data Tantalum Target
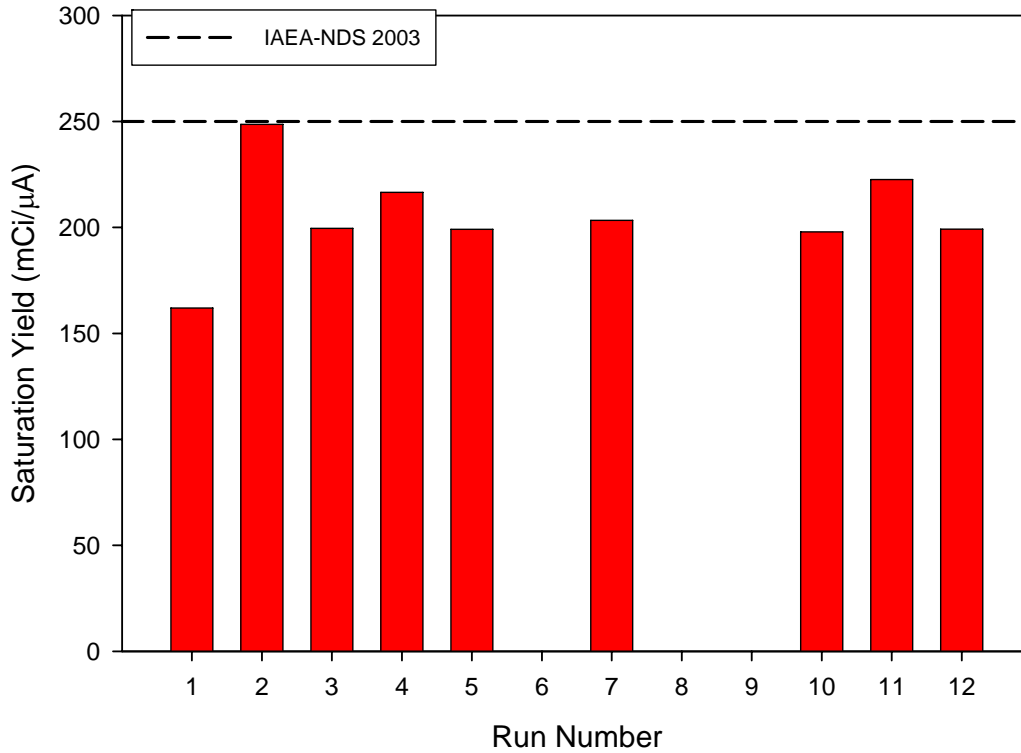

Figure 6-31: TS7-WMC Tantalum Insert ^{18}F Yield Summary

Table 6-8: TS7-WMC Tantalum Insert ^{18}F Yield Summary

Run	Date	Nuclear Reaction	I_{beam} (μA)	IT (min.)	Sat. Yield (mCi/μA)
1	1/12/2008	$^{18}O(p,n)^{18}F$	85	60	162.0
2	1/12/2008	$^{18}O(p,n)^{18}F$	75	25	248.7
3	1/13/2008	$^{18}O(p,n)^{18}F$	75	30	199.6
4	1/13/2008	$^{18}O(p,n)^{18}F$	80	30	216.6
5	1/13/2008	$^{18}O(p,n)^{18}F$	80	60	199.1
6	1/14/2008	$^{18}O(p,n)^{18}F$	80	60	QC1
7	1/14/2008	$^{18}O(p,n)^{18}F$	60	120	203.4
8	1/15/2008	$^{18}O(p,n)^{18}F$	70	60	QC2
9	1/15/2008	$^{18}O(p,n)^{18}F$	75	140	QC3
10	1/15/2008	$^{18}O(p,n)^{18}F$	75	180	197.9
11	1/16/2008	$^{18}O(p,n)^{18}F$	40	30	222.6
12	1/16/2008	$^{18}O(p,n)^{18}F$	70	260	199.2

73

Figure 6-32: 10.5 Ci of ^{18}F in Dose Calibrator

The TS7 system does not offer any significant performance advantage to WMC from a traditional production standpoint. While the net yield is a roughly a factor of two when compared with single target production, the GE targets can be run in a dual irradiation configuration (Figure 6-33). TS7 does, however, offer a unique advantage in the case of long irradiation times. Using the thermosyphon system on the front end of the production schedule could potentially eliminate an extra irradiation and synthesis by running longer than 120 minutes. To make gains over the entire production schedule, a higher intensity target will be needed. Such a target would likely possess chamber dimensions comparable to TS6-WMC, which can exceed dual GE target production for any length irradiation.
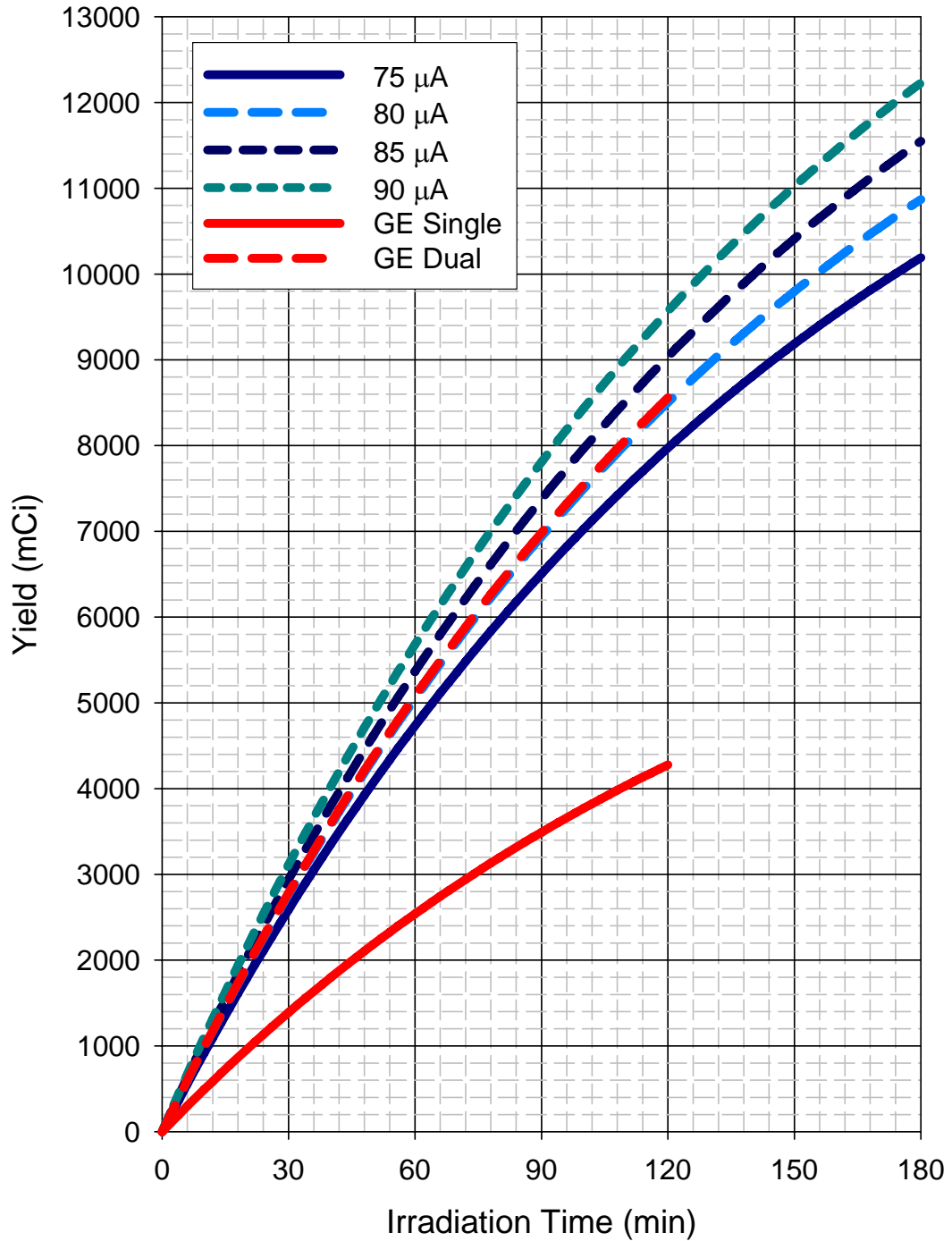
74

TS7 Production Estimates

Figure 6-33: Production Capabilities of TS7-WMC System

75

CHAPTER 7 - CONCLUSIONS

7.1 Summary and Conclusions

Early prototype thermosyphon target systems demonstrated the feasibility of high intensity irradiation via bottom pressurized operation. In the course of evaluating the prototypes, an effective experimental characterization platform was developed. This platform was utilized in parallel with computational modeling efforts[16] to further improve designs. A general control strategy was also developed to provide a simple and robust means of remote target operation.

Cyclotron specific production targets were then designed and implemented in two facilities. These systems were developed with an emphasis on improved heat rejection capabilities as well as increased reliability and serviceability. In both facilities the clinical qualification process has been completed and routine production is underway.

A patent for the Thermosyphon was awarded to Bruce Technologies, Inc. on October 24, 2006 [26]. It is unlikely, however, that any of the targets tested to date have achieved a true thermosyphon mode of operation. The heat transfer behavior is more accurately predicted if a volume averaged boiling mode is assumed rather than a system with distinct boiling and condensing regions. It is not surprising that little phase separation exists due to the combination of a relatively small elevation change in the target chamber and violent boiling process. A larger target would better accommodate the transition from bulk boiling to thermosyphon mode.

Bottom pressurization does, however, offer dramatic improvement in operational stability at high power. This is evident by the gradual onset of penetration in the PETtrace

76

targets. Designing bottom-pressurized targets to operate in a bulk boiling mode could more effectively manage water inventory and will be discussed in the following section.

7.2 Future Work

Bruce Technologies, Inc., is currently developing a 100 µA production target system based on the TS7 platform. The target insert has an inner diameter of 15 mm and will consume approximately 4.7 mL of enriched material per irradiation. Pending analysis at WMC, this system will likely reach the PETtrace retrofit market in late summer 2008. This product will employ an advanced control system that is currently under development at North Carolina State University and Duke.

The advanced target control system is a productized version of the third generation control platform. It features an embedded microprocessor based automation controller with field programmable gate array technology to ensure true deterministic execution. The helium supply system has been redesigned to reduce gas consumption and provide additional state feedback. The target filler employs a pair of two position multi-port rotary valves. These valves are helium operated for radiation hardness and offer electronic position feedback. A diagram of this system is included in Figure 7-1.

A cylindrical target chamber is also currently being developed at North Carolina State University. This concept is designed to take advantage of the bulk boiling regime observed in the PETtrace targets. The target chamber consists of a 17 mm diameter cylinder with surface area equivalent to a 15 mm diameter, 15 mm deep racetrack. This results in a slightly lower volume target than TS6-WMC with almost 4 mm additional depth. Due to the gradual onset of penetration that has been observed, relocating a portion of the condensing region to add

77

depth should improve thermal performance. A drawing of the target insert is included in Figure 7-2.

Finally, continued development of computational models is critical to predicting thermal limit capabilities in untested designs. This effort includes determining the distribution of void for the bulk boiling regime, as well as identifying the transition to a true thermosyphon mode with distinct phase separation.
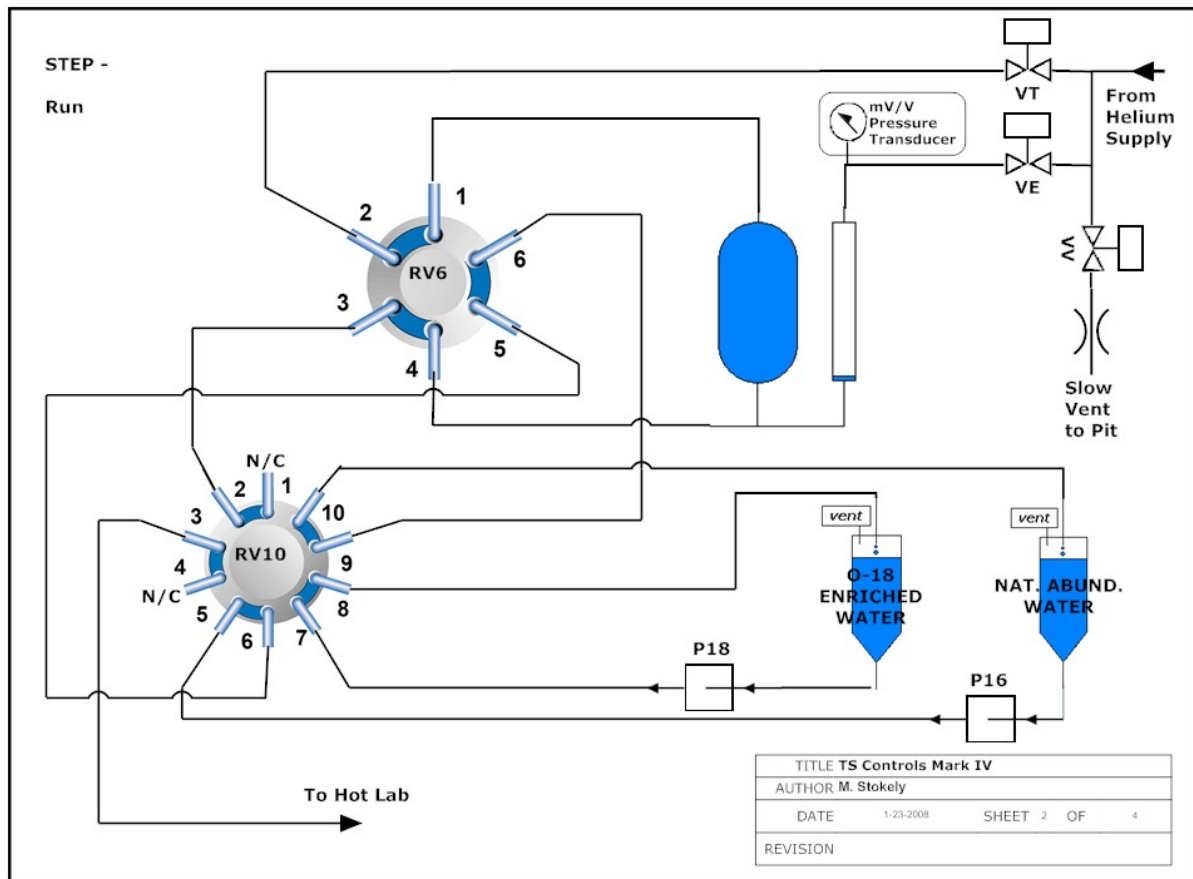

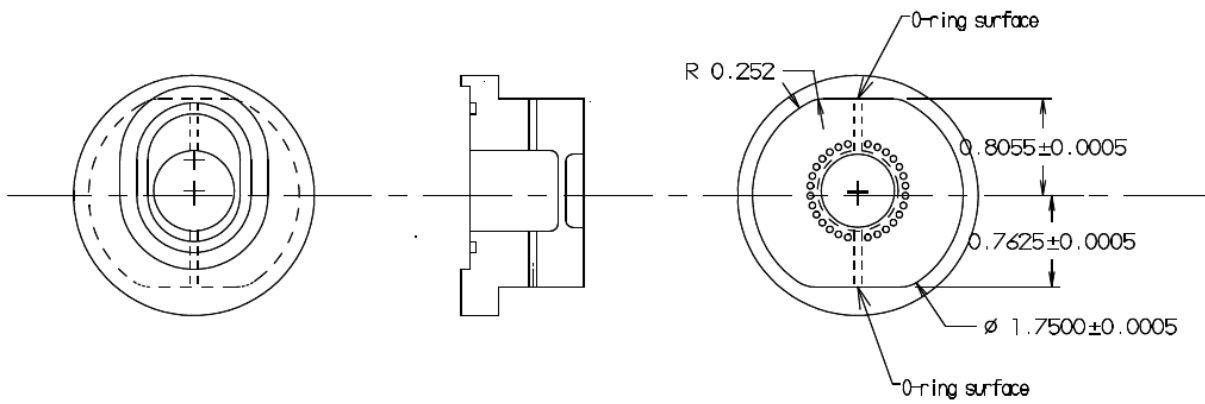**Figure 7-1: Version 4.0 Target Filler Concept**

78

Figure 7-2: Cylindrical Chamber Target Insert

REFERENCES

1. A Incorporated, CFX ANSYS. ANSYS Incorporated, Cannonsburg, PA, 2005.

2. Alvord C.W., Williamson A.C., Graves T.L., and Zigler S.S. <u>Design, test and widespread implementation of a compact kilo-Watt fluoride ion target</u>. *Nuclear Instruments and Methods in Physics Research B*. 241:708-712, 2005.

3. Berridge, M.S., Kjellstrom R. <u>Designs and use of silver [^{18}O] water targets for [^{18}F] fluoride production</u>. *Applied Radiation and Isotopes.* 50:699-705, 1999.

4. Coleman R.E., <u>PET/CT Essentials for Clinical Practice</u>. New York: Springer, 2004.

5. Collier J.G., <u>Convective Boiling and Condensation</u>. UK: McGraw Hill, 1981.

6. "CoolCube." Bio-ChemValve, Inc. <http://www.bio-chemvalve.com/Coolcube.pdf>.

7. Delbeke D., <u>Practical FDG Imaging: A Teaching File</u>. New York: Springer, 2004.

8. Eriksson T., Berstrom J.O., and Norling J. "Using a niobium water target on the PETtrace cyclotron producing ^{18}F." *Proceedings of the Eleventh Workshop on Targetry and Target Chemistry*. Cambridge, UK: 2006.

9. "Havar." Hamilton Precision Metals. <http://www.hpmetals.com/pdfs/Havar.pdf>.

10. Hess E., Takàcs S., Scholten B., Tàrkànyi F., Coenen H. H., and Qaim S. M. <u>Excitation function of the ^{18}O(p,n)^{18}F nuclear reaction from threshold up to 30 MeV</u>. *Radiochimica Acta*. 89:357–362, 2001.

11. Humbert D., Nichols A., and Schwerer, O. IAEA Nuclear Data Section: provision of atomic and nuclear databases for user applications. *Applied Radiation and Isotopes*. 60:311-316, 2004.

12. Kilbourn M.R., Hood J.T., Welch M.J. A simple ^{18}O water target for ^{18}F production. *International Journal of Applied Radiation and Isotopes*. 35:599-602, 1984.

13. Newnam R. High Capacity Heat Exchangers for Recirculating ^{18}F Radionuclide Production Targets. Master of Science Thesis, North Carolina State University. Raleigh, North Carolina: 2007.

14. Nutt R. The History of Positron Emission Tomography. *Molecular Imaging and Biology*. 4:11-26, 2002.

15. Peeples J.L. Design and Optimization of Thermosyphon Batch Targets for Production of ^{18}F. Master of Science Thesis, North Carolina State University. Raleigh, North Carolina: 2006.

16. Peeples J.L. Design and Testing of Thermosyphon Batch Targets for Production of ^{18}F. Doctor of Philosophy Dissertation, North Carolina State University. Raleigh, North Carolina: 2006.

17. Phelps M.E. PET: Molecular Imaging and Its Biological Applications. New York: Springer, 2004.

18. Roberts, A.D., Daniel, L.C., Nickles, R.J., 1995. A high power target for the production of [^{18}F]fluoride. *Nuclear Instruments and Methods in Physics Research B*. 99:797–799, 1995.

19. Roberts A.N., <u>Thermosyphon Targets Designed for the Production of ^{18}F for Use in Positron Emission Tomography</u>. Master of Science Thesis, North Carolina State University. Raleigh, North Carolina: 2002.

20. Sajjad M., Lambrecht R.M., and Wolf A.P. <u>Investigation of Some Excitation Functions for the Preparation of ^{15}O, ^{13}N and ^{11}C</u>. *Radiochimica Acta.* 36:159-166, 1984.

21. Satyamurthy N., Amerasekera B., Alvord C.W., Barrio J.R., and Phelps M.E. <u>Tantalum [^{18}O]Water Target for the Production of [^{18}F]Fluoride with High Reactivity for the Preparation of 2-Deoxy-2-[^{18}F]Fluoro-D-Glucose</u>. *Molecular Imaging and Biology*. 4:65-70, 2002.

22. SigmaPlot, 2002. Sigma Plot$^{®}$ version 9.0. SPSS Publishing, Chicago, Illinois.

23. Strangis R. and Lepera C.G. "Reliable Fluorine-18 [^{18}F^{-}] Production at High Beam Power." *18th International Conference on Cyclotrons and their Applications.* Giardini Naxos, Italy: 2007.

24. Stokely M.H. <u>Advanced Thermosyphon Targets for Production of the ^{18}F Radionuclide</u>. Master of Science Thesis, North Carolina State University. Raleigh, North Carolina: 2007.

25. Stokely M.H., Bida G., Doster J. M., and Wieland B.W. "Correction Factor to Obtain Thick Target Yields for $H_2^{18}O(p,n)^{18}F$ from $^{18}O(p,n)^{18}F$," *Proceedings of the Eleventh Workshop on Targetry and Target Chemistry*. Cambridge, UK: 2006.

26. Wieland B.W. (2006). *U.S. Patent No.* 7127023. Washington, DC: U.S. Patent and Trademark Office.

27. Wieland B.W., Bida G., Padgett H., Hendry, G., Zippi E., Kabalka G., Morelle J., Verbruggen R., and Ghyoot M. In-target Production of [^{13}N]Ammonia via Proton Irradiation of Dilute Aqueous Ethanol and Acetic Acid Mixtures. *Applied Radiation and Isotopes*. 42:1095-1998, 1991.

28. Wieland B.W. and Wolf A.P. Large Scale Production And Recovery Of Aqueous F-18 Fluoride Using Proton Bombardment Of A Small-Volume [^{18}O]Water Target. *Journal of Nuclear Medicine.* 24:122, 1983.

29. Wieland B.W., Wright B.C., Bida G.T., Illan C.D., Doster J.M., Clark J.C., and Runkle R.C. "Thermosyphon Batch and Regenerative Turbine Recirculating ^{18}O$(p,n)^{18}$F Water Targets for Operation at High Beam Power," *Proceedings of the Tenth Workshop on Targetry and Target Chemistry*. Madison, WI: 2004.